Chem Soc Rev

Dynamical Resonances in Chemical Reactions

Dynamical Resonances in Chemical Reactions

Tao Wang[1], Tiangang Yang[1], Chunlei Xiao[1,*], Zhigang Sun[1,*], Donghui Zhang[1,*], Xueming Yang[1,2*], Marissa L. Weichman[3,†,*] and Daniel M. Neumark[3,4,*]

[1]State Key Laboratory of Molecular Reaction Dynamics, Dalian Institute of Chemical Physics, Chinese Academy of Sciences, 457 Zhongshan Road, Dalian, Liaoning 116023, China

[2]Department of Chemistry, Southern University of Science and Technology, 1088 Xueyuan Road, Shenzhen 518055, China.

[3]Department of Chemistry, University of California at Berkeley, Berkeley, CA 94720, USA

[4]Chemical Sciences Division, Lawrence Berkeley National Laboratory, Berkeley, California 94720, United States

*Email addresses:
chunleixiao@dicp.ac.cn
zhangdh@dicp.ac.cn
xmyang@dicp.ac.cn
marissa.weichman@jila.colorado.edu
dneumark@berkeley.edu

[†]Present address: JILA, National Institute of Standards and Technology, Boulder, Colorado 80305, USA

Abstract

The transition state is a key concept in the field of chemistry and is important in the study of chemical kinetics and reaction dynamics. Chemical reactions in the gas phase are essentially molecular scattering processes, which are quantum mechanical in nature. Thus probing and understanding detailed quantum structure in the transition state region of chemical reactions, such as reactive resonances, is a central topic in this field. In this article, we focus on recent progress in the study of resonances in elementary bimolecular reactions using state-of-art transition state spectroscopy methods: high-resolution photoelectron spectroscopy and quantum state specific backward scattering spectroscopy. The experimental results are compared with high-level quantum dynamics calculations based on highly accurate potential energy surfaces. The dynamics of reactive resonances are also interpreted based on scattering wavefunctions obtained by time-dependent wavepacket calculations. Here, we review many systems that illustrate how reactive resonances can strongly influence the dynamics of elementary chemical reactions.

Keywords：transition state, reactive resonance, Feshbach resonance, shape resonance, potential energy surface, high-resolution photoelectron imaging, quantum state specific backward scattering spectroscopy.

I.   Introduction

Resonances are ubiquitous in both classical and quantum systems. In atomic and molecular systems, when the energy of a photon equals the energy difference between two quantum mechanical states, the photon can be resonantly absorbed. The absorption spectrum correspondingly shows a resonance peak, and the width of this peak can be related to the lifetime of the states involved. Resonance phenomena have also been detected in particle scattering processes in nuclear physics. In the 1930s, Fermi and collaborators noticed elevated cross sections for slow neutron scattering at certain energies,[1,2,3,4] which were interpreted by Bethe[5] and Bohr[6] as particle scattering resonances due to certain quasi-stable states of the collision complex. These elementary particle resonances have been crucial for the understanding of the fundamental forces of nature. Scattering resonances have also been discovered in electron-heavy particle scattering processes.[7,8,9] Resonances also exist in inelastic atomic and molecular collisions. As gas-phase chemical reactions are in essence atomic and molecular scattering processes, resonant phenomena have been an important topic in the study of the dynamics of chemical reactions over the last few decades.

In a chemical reaction, reactants pass through a transition state region along the reaction coordinate between reactants and products, where chemical bonds are broken and reformed. This transition state, first proposed by Polanyi and Eyring in the early 1930's,[10,11,12] dictates almost every aspect of a chemical reaction, and has played a central conceptual role in the development of chemistry as a branch of science. Therefore, observing and understanding the transition state have been regarded as the "Holy Grails" of chemistry.[13,14]

In the transition state region of a chemical reaction, there can exist quantum resonance states which sometime dominate reaction dynamics. We can use a one-dimensional model of a chemical reaction (Figure 1) to illustrate the concept of the transition state and reactive resonances.[15] In a typical chemical reaction with a simple energy barrier (Figure 1a), the transition state is traditionally defined as the region near the top of the energy barrier. In this model system, the barrier simply acts

as a bottleneck for chemical reaction, and the reaction probability increases monotonically to a plateau value as the reaction energy goes above the barrier (Figure 1b). In some cases, however, quasi-bound quantum states can exist in a peculiar adiabatic potential wells along the reaction coordinate, as shown in Figure 1c. These transiently trapped quantum states are called reactive or dynamical resonance states, and normally live from a few tens to hundreds of femtoseconds (Figure 1d). The presence of such features can significantly enhance the reaction probability through resonance-mediated tunneling, as seen clearly in the calculated reaction probability in Figure 1d. However, directly detecting the structure and dynamics of these reaction resonances is a great experimental challenge.

Two primary experimental methods have been developed and applied to probe reactive resonances in bimolecular reactions: anion photoelectron spectroscopy (PES) and high-resolution crossed molecular beam scattering. Using anion photoelectron spectroscopy, photodetachment of a bound anion similar in geometry to the desired neutral transition state can yield a spectrum showing structure very sensitive to the shape of the neutral potential energy surface. Given sufficient energy resolution, the geometry, energetics, and vibrational frequencies of the transition state can be illuminated, as well as the positions and spectral widths of resonances bound or quasi-bound along the reaction coordinate. Using high-resolution crossed molecular beam scattering, one can obtain product quantum state-resolved scattering patterns, which can be used to trace the dynamics of reactive resonances. By focusing specifically on the backward scattered products, one can determine the energy and lifetime of reaction resonances.

In recent years, significant progress has been made in both the experimental and theoretical study of reactive resonances, and there have been several comprehensive reviews published on this topic.[13,16,17,18,19,20,21,22] In this review, we will provide a brief summary of the basics and experimental methods in this area of research (Section II), discussion of recent measurements of reactive resonances in several benchmark systems (Section III), and implications for future work (Section IV).

II.   Development of New Experimental Methods

Resonances in bimolecular chemical reactions are difficult to probe experimentally due to their short (typically few-femtosecond) lifetimes and their low number densities. Furthermore, because it is not possible to precisely initiate a bimolecular reaction on a femtosecond time scale, conventional ultrafast spectroscopy methods cannot easily be applied to investigate reactive resonances. Over the last few decades, two experimental methods, anion photoelectron spectroscopy and high-resolution crossed molecular beam scattering have elevated understanding of reactive resonances, in conjunction with accurate quantum dynamics theory.

II.1) Anion Photoelectron Spectroscopy

Anion photoelectron spectroscopy is a powerful tool to study the vibrational and electronic structure of transient neutral species through photodetachment of a stable negative anion.[23] Experimentally, a packet of mass-selected anions, A^-, is irradiated with light. A photoelectron may be detached if the photon energy exceeds the binding energy of the electron:

$$A^- + h\nu \rightarrow A + e^- \tag{1}$$

The photon energy $h\nu$ is conserved between the binding energy of the final neutral state (eBE) and the kinetic energy of the outgoing photoelectron after detachment (eKE) according to:

$$eBE = h\nu - eKE \tag{2}$$

The eKE distribution is measured, and can show discrete features corresponding to detachment to specific neutral electronic and vibrational quantum states. The resulting photoelectron spectra are typically plotted in eBE, as this quantity is independent of the choice of photon energy.

Anion PES is one of the few ways to spectroscopically access neutral transition states on unimolecular and bimolecular reactive surfaces.[24] Photodetachment of a bound anion similar in geometry to a relevant part of the neutral reactive surface can provide a direct spectroscopic probe of Franck-Condon (FC) structure in modes perpendicular to the reaction coordinate[25,26] as well as sharper features corresponding to discrete reactive resonances lying along the reaction coordinate (Figure 2).[27] Analysis of transition state spectra can therefore reveal detailed information about the geometry, vibrational frequencies, energetics, and resonances of the transition state and reactant and product complexes. By extension, characterization of short-lived quantized states in the transition state region provides a wealth of information about how the reactive surface governs chemistry.

In recent years, anion PES has made significant progress in transition state spectroscopy because of the development of a high-resolution variant of this technique, slow photoelectron velocity-map imaging of cryogenically-cooled anions (cryo-SEVI). The cryo-SEVI technique has been discussed extensively elsewhere.[28,29,30,31] Anions are photodetached with a tunable laser at various fixed wavelengths, and the kinetic energy distribution of the resulting photoelectrons is measured with a velocity-map imaging (VMI) lens. Energy resolution is optimized by carrying out photodetachment very close to threshold, and by using low VMI extraction voltages to magnify the photoelectron image and selectively detect the slowest electrons. By tuning the detachment laser above each spectral feature of interest, the entire spectrum can be acquired in high-resolution energy windows. Under these conditions, SEVI can achieve instrumental energy resolution down to a wavenumber. With cryo-SEVI, the anions are collisionally cooled with cold, inert buffer gas in a radiofrequency ion trap before photodetachment, allowing thermalization to their ground vibrational and electronic states.[27] This method has demonstrated complete suppression of hot bands and dramatically narrowed rotational envelopes for detachment of molecular anions. Ion temperatures as cold as 10 K and spectral peak widths as narrow as 2-3 cm^{-1} have been reported for molecular

systems.[27,29, 32] Photodetachment of cold ions is particularly advantageous for resolving resonances in a transition state spectroscopy experiment, as one avoids the averaging over angular momentum partial waves found in crossed beam scattering experiments.

The new capabilities of cryo-SEVI have allowed for exquisite spectral characterization of many systems that were previously not feasible. Its applications for transition state spectroscopy have been recently demonstrated through the study of reactive resonances in the benchmark $F + H_2$ reaction, the five-atom $F + CH_4$ reaction, and the seven-atom $F + CH_3OH$ reaction, all of which will be discussed further below. In these systems, resonance features are newly resolved, serving as excellent points of comparison for state-of-the-art theoretical treatment of bimolecular reactive surfaces, as well as with high-resolution crossed molecular beam scattering results.

II.2) State-Resolved Crossed Beam Reactive Scattering with Backward Scattering Spectroscopy

High-resolution crossed molecular beam scattering experiments have also been a key method in the study of elementary chemical reaction dynamics. In a crossed molecular beam scattering experiment, two beams are crossed in a high vacuum chamber at a specific collision energy, and the resulting reaction products are scattered in different directions.[33] Various detection methods have been applied to detect reaction products and to measure their scattering patterns. These scattering patterns can report on the reaction dynamics, and in certain cases can demonstrate evidence of reactive resonances at certain collision energies via features like forward scattered peaks. However, important properties of reactive resonances, such as the resonance energy and lifetime, cannot be directly determined. We rely solely on theoretical dynamics calculations to obtain these crucial information.

A significant complication in using crossed beam scattering to probe reactive resonances is the partial wave averaging effect. In a typical reactive scattering event,

the product scattering pattern is the result of many partial waves with different total angular momentum J. The signatures of reactive resonances in the scattering pattern can be easily smeared out by averaging over many different partial waves, and thus important properties such as the resonance state energy and lifetime are not possible to measure experimentally at a specific collision energy. Partial wave averaging makes it very difficult to observe many resonances in a total cross section measurement as a function of collision energy, which would be the most intuitive way to see them.[34] However, one can look at the back-scattered signal as a function of collision energy, where averaging effects are mitigated for reasons discussed further below.

In recent years, various high-resolution crossed molecular beam techniques have been developed and applied for the improved study of elementary chemical reactions. Crossed beams methods are designed to measure scattering reaction product flux intensities from the crossing region at different scattering angles, which let us to determine the differential cross sections (DCS). Yang and co-workers have developed the quantum state specific backward scattering spectroscopy method,[35,36] where reactive scattering differential cross sections are measured in the backward direction with quantum state resolution as a function of collision energy. The efficacy of this method is based on the principle that in a hard sphere scattering process, backward scattered products are formed through collisions with impact parameters near $b \approx 0$. This principle is also applicable to molecular reactive scattering processes, in which backward scattered products are primarily formed from scattering with low J partial waves. Since the signatures of reactive resonances are most clear in the low J partial wave scattering, directly measuring the backward scattering differential cross section as a function of collision energy can provide the most sensitive probe of reactive resonances. This method can be used to measure both the position and lifetime of the resonance state. In the last decade or so, this approach has been successfully applied to study reactive resonances in benchmark systems such as $F+H_2$ and $Cl+H_2$, in combination with the high-resolution H-atom Rydberg tagging technique.

8

The high-resolution H-atom Rydberg tagging time-of-flight (HRTOF) technique was developed by Welge and co-workers[37,38,39] and has been widely applied in the Davis and Yang groups[40,41,42,43,44,45] for the study of elementary chemical reactions. The central scheme of this technique is the two-step efficient excitation of an H or D atomic product from its ground state to a long-lived high-n Rydberg state without ionization. These "tagged" neutral H or D atoms fly free of space charge and stray field effects, and are field-ionized at the end of the TOF before detection with microchannel plates.

In comparing the methods outlined in II.1 and II.2, note that, depending on the anion geometry, anion photoelectron spectroscopy can be sensitive to quantized resonance structure in the entire transition state region on either side of the barrier, while crossed beam scattering experiments can only detect those resonance states that have significant influence on the reaction dynamics of bimolecular reaction processes. It is of great interest to relate the two experimental methods and identify the features observed in anion PES that manifest in scattering experiments.

III.   Resonances in Chemical Reactions

The contributions of molecular beam scattering and anion PES experiments to the search for reactive resonances and transition state structure is well demonstrated through the history of the benchmark F + H_2 reaction. In the 1970s, reactive resonances were theoretically predicted in the F + H_2 reaction on two-dimensional potential energy surfaces for collinear reactions.[46,47,48,49] Theoretical results showed a sharp Lorentzian-like peak in the total integral cross section as a function of collision energy, a clear signature of a reactive resonance, but the physical origin of this resonance was not clarified. In 1985, Lee and coworkers performed a milestone crossed beam experiment on the F + H_2 reaction with vibrational state resolution of the HF products.[50,51] The HF(v'=1,2) products were mainly backward scattered, while a clear forward-scattering peak for the HF(v'=3) product was observed (Figure 3) and initially attributed to a reactive resonance. Forward scattering for the DF(v'=4)

product of the F + D_2 reaction as well as the HF(v'=3) product of the F + HD reaction were also reported.[52] However, both quasi-classical trajectory (QCT) calculations[53] and quantum mechanical scattering studies[54] on the Stark-Werner potential energy surface (SW-PES)[55] show forward scattering peaks of HF(v'=3), with the peak of the quantum calculations larger than the classical calculations. This implies that the HF(v'=3) forward scattering peak may be of classical origin. In 1993, Neumark and coworkers carried out transition state spectroscopy experiments via photodetachment of FH_2^- anions, and observed a progression of bending levels of the FH_2 transition state complex, but saw no signs of sharp reactive resonances from trapped states along the reaction coordinate.[56,57]

In 2000, Liu and coworkers reported a crossed molecular beam scattering study of the F + HD reaction measuring the excitation function, or integral cross section as a function of collision energy, with quantum dynamics calculations carried out on the SW-PES.[58] A clear step structure in the excitation function of the HF + D product channel was observed around 0.5 kcal/mol (Figure 4a). This step-like feature was reproduced by quantum dynamics calculations, but not by QCT calculations, suggesting that this structure is purely a quantum phenomenon. Further analysis shows that this feature is due to a single reactive resonance. In contrast, the excitation function of the DF + H channel shows no resonant features (Figure 4b). Features were also observed in the F + H_2 and F + D_2 reaction excitation functions,[59] and theoretical results based on the SW-PES predicted the existence of a resonance in the F + H_2 reaction.[60,61] These results raised intriguing questions about the differences in dynamics of these reaction isotopologs.

More recently, resonances in the F + H_2 and F + HD reactions have been further investigated using high-resolution crossed beams scattering method and more accurate dynamics theory to undertsand the accurate quantum dynamics of resonances in these isotopologs. [62,63,64,65,66] Scattering resonances involving vibrationally excited reactants, such as F + HD(v=1) and Cl+H_2, have also been studied. [67,68] Resonances in the F+H_2(D_2) reactions have also been investigated using the cryo-SEVI

method.[69,70] In addition, resonances in much more complex polyatomic reaction systems, such as the F+CH_4 reaction and the F + CH_3OH reaction, can now be experimentally investigated with the same technique.[71,72] These studies have pushed our understanding of reaction resonances to a much higher level. In the following sections, we will provide a comprehensive review of these new developments.

III.1) Probing Reactive Resonances in the F+H_2 Reaction using Cryo-SEVI Spectroscopy

The recently improved capabilities of cryo-SEVI transition state spectroscopy are perhaps best-illustrated for the F + H_2 → H + HF reaction. This system represents a fairly ideal case for anion PES transition state spectroscopy, as the corresponding FH_2^- anion is bound and has similar bond lengths to the neutral transition state, providing good Franck-Condon overlap (Fig. 5). However, FH_2^- is linear while the F + H_2 transition state is bent. As a result, the photoelectron spectrum is dominated by an FC progression in the H-H hindered rotor (or F-H-H bending states) of the FH_2 transition state complex. An early anion photoelectron spectrum of F + H_2 resolved this bending progression.[56]

Improved photodetachment simulations later indicated that sharp features corresponding to bound and quasi-bound resonances in the F + H_2 reactant and product van der Waals (vdW) wells should be visible in a photoelectron spectrum with 1 meV resolution.[73] Traditional anion PES methods lacked the energy resolution to observe these features. The poor threshold photodetachment cross section of the FH_2^- anion also made a study using zero electron kinetic energy spectroscopy intractable. The first SEVI study of FH_2^-, before cryogenic anion cooling was incorporated into the instrument, showed a hint of a predicted product resonance.[69]

Recently, Neumark and coworkers returned to the F + H_2 reaction and its fully deuterated isotopolog with the cryo-SEVI technique,[70] allowing for unambiguous resolution of resonances in the product and reactant wells and near the transition state. The reaction of F with *para*-H_2 (*p*-H_2) was investigated in particular, as spectral

congestion is reduced and the resonances are predicted to be more pronounced than in the *normal*-H_2 (n-H_2) case. *para*-FH_2^- and n-FD_2^- ions were synthesized by introducing F^- into the cryogenic ion trap and allowing clustering with p-H_2 or n-D_2 buffer gas, respectively. This method produced substantially higher ion yields than a molecular beam ion source, and proved essential for achieving the required high signal-to-noise ratio needed to discern small resonance features on top of intense broader features. The resolution and sensitivity of the measurements was also much enhanced via improvements in image acquisition and processing, to better reproduce weak resonance features on top of broad signal.[74]

Cryo-SEVI spectra for p-FH_2^- and n-FD_2^- are shown in Figures 6a and 6b, with overview traces in green, and high-resolution traces in purple. Theoretical spectra calculated by Alexander and Manolopoulos are also shown (red and blue traces), making use of newly developed high-quality potential energy surfaces.[75] For both FH_2^- and FD_2^-, excellent agreement between the experimental and calculated spectra has been achieved. The calculated scattering wavefunctions at the energy of each peak can also be extracted to aid in the state assignments of observed features. The neutral wavefunctions corresponding to labeled spectral peaks are shown in Figure 7 in red and blue, with the initial anion wavefunctions shown in green.

The broad features A, B, and C in the FH_2^- spectrum and peaks D and E in the FD_2^- spectrum have been detected previously and assigned to the H-H(D-D) hindered rotor direct scattering states. Several additional features are newly observed. For $FH_2^{-,-}$ peak a, lying just slightly above peak A, is clearly resolved, as is peak α, which manifests experimentally as a shoulder on the low-eBE side of peak A. Both a and α are well-reproduced in the calculated spectrum as sharp resonances. For FD_2^-, two weak features, peaks b and c, are observed at low eBE and also manifest clearly in the simulation.

The nature of these resonance features is unambiguously revealed by their localization and nodal structure in the wavefunction plots in Figure 7. Peak A had previously been assigned to a delocalized direct scattering state, but it is now clear that

it is in fact a quasibound resonance localized at the $F + H_2$ transition state, with three quanta of excitation in the H-F stretching mode. Peaks a, b, and c are quasibound resonances supported by the H···H-F (D···D-F) product vdW well in the exit channel, with different quanta in the H-F (D-F) and H-HF (D-DF) stretching modes, while peak α is a resonance supported by the F···H_2 vdW reactant well in the entrance channel. This resonance was predicted and analyzed for the first time by the time-independent Q-matrix method.[76] Peak a was predicted by Russell and Manolopoulos in 1996,[73] but peaks b and c in the FD_2^- spectrum were not previously predicted or observed. The fact that there are two resonances supported in the D···D-F product well, yet only one resonance in the H···H-F well is simply a consequence of the reduced mass difference of the two isotopologs.

The experimental positions, widths, and intensities of these newly resolved reactive resonances are exquisite probes of the $F + H_2$ transition state region, and make an exceptional point of comparison with theory. The experimental results can be used to quantitatively benchmark the quality of calculated FH_2^- anion vibrational wavefunctions and neutral reactive surfaces.

III.2) Probing Resonances in the $F + H_2$ Reaction using State-Resolved Crossed Beams Scattering

In-depth studies of the $F + H_2$ reaction using high-resolution crossed beam backward scattering spectroscopy in combination with state-of-the-art quantum dynamics calculations have also helped to reveal the true physical nature of reaction resonances in this benchmark system. In this section, we will describe the new advances in this system, starting from the $F + H_2(v=0, j=0)$ reaction.

Experiments on the $F + H_2(v=0, j=0)$ reaction were carried out by Yang and co-workers using crossed beam reactive scattering in combination with H-atom Rydberg tagging detection.[62] A beam of cryogenic *para*-H_2 in only the $j=0$ state was obtained by cooling the beam source with liquid nitrogen. TOF spectra of the

hydrogen atom reaction products were measured in a range of scattering angles at the collision energy of 0.52 kcal/mol. From conservation of energy and momentum in the scattering process, HF product rovibrational state-resolved differential cross sections were determined. Figure 8a shows the experimental three dimensional product DCS contour plot. A pronounced forward scattering peak for the HF(v'=2) product, which was not observed previously by Lee and coworkers[51] in the collision energy range of 0.7 to 3.4 kcal/mol was clearly detected. Full quantum scattering calculations based on an accurately constructed potential energy surface, XXZ-PES,[63] were carried out (Figure 8b). The excellent agreement between experiment and theory provides a solid basis for understanding the dynamics of resonances for this reaction.

Figure 9 shows the calculated total reaction probabilities for the F + H$_2$(v=0,j=0) reaction as a function of collision energy for the J=0 partial wave. It is clear that there are two reaction resonance states in the low energy region, lying at collision energies of 0.26 and 0.46 kcal/mol on the XXZ-PES. Dynamical analysis indicates that the pronounced forward scattering of the HF(v'=2) product is enhanced by the constructive interference of these two resonance states. At a collision energy of 0.52 kcal/mol, the contribution of the first resonance (see Fig. 9) to the cross section is in the partial wave range J= 5-11, while the contribution of the second one is in the range J=0-4 on the XXZ-PES.[62] Note that the two resonances cross at different partial waves on different potential energy surfaces.[77] The J=0 wave function of the ground state resonance shows the existence of three nodes along the H-F coordinate in the HF-H' complex with no nodes along the reaction coordinate (Figure 10A). This state is therefore the ground resonance state supported by the v=3 adiabatic potential of the exit channel, and is labelled (v_1=0,v_2=0,v_3=3), where v_1 is the quantum number for the H-HF stretching mode, v_2 the bending mode, and v_3 the HF stretching mode. The second resonance state (J=0) at 0.46 kcal/mol exhibits three nodes along the H-F coordinate in the HF-H' complex with one node along the reaction coordinate (Figure 10B). This resonance state can be assigned to the (103) resonance state with one quantum of vibrational excitation along the reaction coordinate in the v=3 adiabatic

potential of the exit channel.[62]

Figure 11 shows the resonance-mediated reaction mechanism in a one-dimensional vibrationally adiabatic picture.[62] The HF(v'=3)-H' vibrational adiabatic potential (VAP) well has a deep well in the post barrier region as well as a shallow vdW well. The one-dimensional wave function for the ground resonance state shows that this state is mainly trapped in the inner deep well of the HF(v'=3)-H' VAP with almost no vdW character, while the excited resonance wave function is mainly a vdW resonance. The collision energy 0.52 kcal/mol is well below the reaction barrier, indicating that the reaction takes place through a post-barrier, resonance-enhanced tunneling mechanism. In addition, the main product is HF(v'=2), rather than HF(v'=3). The resonance states are trapped in the HF(v'=3)-H' VAP and decay to the HF(v'=1, 2) product channels via strong couplings between HF(v'=3)-H' and HF(v'=1, 2)-H' adiabatic curves.

The HF(v=3) channel was investigated in a similar high-resolution crossed beam experiment to understand the nature of the forward scattering at higher collision energies.[78] The excitation function of the HF(v'=3) channel from 0.4 to 1.2 kcal/mol shows that the threshold of the HF(v'=3) channel is around 0.52 kcal/mol, indicating that this channel has no significant exit barrier for reaction, in good agreement with the quantum dynamics calculations. If the reaction energy is below the threshold for the HF(v'=3) channel, the resonance-trapped complex decays into the lower HF(v'=2, 1, 0) channels.

Because the centrifugal potential makes the effective potential well increasingly shallow as total J increases, the HF(v'=3)-H' product well cannot support the excited resonance state at higher J. Theoretical analysis shows that the ground resonance state can form the HF(v'=3) product via tunneling through the centrifugal barrier via a shape resonance mechanism.[78] This shape resonance mechanism can only happen in a narrow collision energy range, from 0.60 to 0.85 kcal/mol. For total J >10, no resonance state can be supported on the effective potential, thus a slow-down type mechanism dominates the formation of HF(v'=3) over the exit centrifugal barrier,

similar to the time-delay mechanism in the H + HD reaction.[79,80,81] This suggests that the HF(v'=3) forward scattering at higher collision energies is related to the adiabatic potential involved in the resonance, but not induced by a specific resonance state. Shape resonances have also been observed in the reaction of $S(^1D_2)$ + H_2 using the crossed beam method.[82,83] Previous theoretical studies using time independent Q-matrix calculations[84] show that the resonance contributes to the differential cross sections of the HF(v'=3) product until about J=20. Resonance contributions to the differential cross section at the collision energy of 1.5 kcal/mol were also analyzed by the Regge Pole Theory.[77] While this work appears to draw different conclusions than the results shown in ref. 78, the slowdown mechanism at high J described above and the resonance mechanism are hard to distinguish in these analyses.

In the F+H_2 reaction, there are also long lived vdW resonance states that have been predicted and analyzed on the FXZ PES.[76,84] Similar structures are also seen in the F+HD reaction.[85,86] However, these resonances have yet to be observed in a crossed beams experiment, most likely because they are usually too sharp to be detected with backward scattering spectroscopy, which has limited energy resolution relative to the narrow width of vdW resonances. In addition, these sharp resonances are also mixed with the direct reaction channel, making them very difficult to detect in experiment.

III. 3) Isotope Effects and Partial Wave Resonances in the F + HD → FH + D Reaction

The energies and lifetimes of reactive resonance states, and thus the reaction dynamics, can be affected by isotope substitution effects. For instance, it is well known that the F + HD → HF + D reaction behaves quite differently from the F + H_2 → HF + H reaction. Illuminating the dynamical differences between isotopolog systems would aid in understanding resonance isotope effects and thus also the nature of reactive resonances. The F + HD → HF + D reaction has thus been reinvestigated using the high-resolution D-atom Rydberg tagging TOF method.[64] The quantum

state-resolved differential cross sections have been measured for this reaction in the collision energy range of 0.3 to 1.2 kcal/mol and are shown in Figure 12. The most striking observation is the dramatic variation of the DCS around the collision energy of 0.5 kcal/mol.

Quantum state-resolved differential cross sections of the F + HD → HF + D reaction have also been measured in the backward scattering direction for the collision energy range of 0.2 – 1.2 kcal/mol.[64, 65] Figure 13 shows the backward scattering DCS of the HF(v'=2, j'=0-3) product of the F + HD → FH + D reaction as a function of collision energy, a clear peak in the experimental spectrum is observed at 0.39 kcal/mol and is attributed to a reactive resonance, which is the lowest resonance in the F + HD → HF + D reaction. Quantum dynamics calculations on the XXZ-PES and a more recent FXZ-PES for this reaction have also been performed and compared with the experimental results.[64] Though the theoretical results based on the XXZ-PES agree well with the experimental differential cross sections of the F + H$_2$ reaction at 0.52 kcal/mol, the calculated peak in Figure 11 for the F + HD reaction appears at higher collision energy relative to the observed peak position in the backward scattering DCS spectrum, suggesting that this potential surface is not sufficiently accurate to describe this resonance. In contrast, the calculated resonance peak position based on the FXZ-PES is in much better agreement with the experimental result. For total angular momentum $J = 0$, the calculated energy for this resonance state is 0.40 kcal/mol, very close to the observed peak position of 0.39 kcal/mol. In addition to the peak position, the width of the resonance peak is also in very good agreement with the experimental result. The excellent agreement between the experiment and the most accurate dynamics theory also suggests that quantum state-resolved backward DCS spectroscopy can indeed provide detailed spectroscopic information on the resonance state. From the 0.15 kcal/mol width of the resonance peak, the resonance state lifetime is determined to be about 100 fs for the J=0 partial wave, in good agreement with the theoretically calculated value. This again suggests that backward scattering spectroscopy can provide accurate information on the lifetime of resonance states.

Excellent agreement between experimental results and quantum dynamics calculations on the FXZ-PES have also been achieved in a very small collision energy range with dramatic DCS variations.[64,65] Theoretical analysis reveals that the HF(v'=3)-D adiabatic well is deeper by about 0.3 kcal/mol on the FXZ-PES than on the XXZ-PES (Figure 14). This results in the ground resonance state energy being 0.16 kcal/mol lower when calculated with FXZ-PES for the F + HD reaction. The reason that XXZ-PES agrees well with the F + H$_2$ reaction but not the F + HD reaction is that for F + H$_2$, the results at 0.52 kcal/mol are dominated by the excited resonance state, which is similar on the XXZ-PES and FXZ-PES. There are also other potential energy surfaces available for the system, such as the LWAL-PES, which reproduces the FH$_2^-$ anion photoelectron spectrum better than the FXZ-PES, and the CSZ-PES, which further refines the FXZ-PES.[66, 87] Recently, a comprehensive comparison among FXZ, CSZ, SW and LWAL PESs for the F+HD reaction dynamics has been given; the theoretical results are also compared with the available crossed molecular beam data.[88]

For a longer lived resonance state as in the F + HD → HF + D reaction, rotational structure could be well resolved. Yang and co-workers carried out a high-resolution crossed beam experiment, using quantum state specific backward scattering spectroscopy, to detect the fine rotational structure of reactive resonances.[89] In order to achieve higher TOF resolution as well as a narrow collision energy distribution, both beam sources (F and HD) were cooled to liquid nitrogen temperature. Figure 15 shows the backward experimental (solid circles) and theoretical (red curve) scattering DCS of the HF(v'=2, j'=6) product of the F + HD(j=0) reaction. Clear oscillatory structures are observed and are attributed to partial wave Feshbach resonance structures with J = 12, 13 and 14. These fine oscillation structures observed are essentially the rotational states of transient resonances, observed here for the first time.

III.4) Resonances in Reactions with Vibrationally and

Rotationally Excited Reagents

III.4.1) Resonances in the F + HD(v=1) Reaction

In the previous sections, we have described recent advances in the study of reactive resonances in the reactions of the F atom with ground state H_2 and HD molecules. It is well known that vibrational excitation of reactants has a profound effect on the chemical reaction dynamics and reactivity.[90] For example, enhanced reactivity and bond-selectivity have been observed in the H + H_2O (HOD, D_2O) reactions when reactants are vibrationally excited.[91,92,93,94] Recently, Liu and coworkers have also studied how vibrational excitation affects polyatomic reactions, specifically F/Cl + CH_4 and their isotopologs.[95,96,97] It is worth investigating how reactant vibrational excitation affects reactive resonances.

Recently, Yang and coworkers have studied the F + HD(v=1) reaction using the D-atom Rydberg tagging crossed beams technique with backward scattering spectroscopy.[67] Vibrationally excited HD(v=1, j=0) molecules were prepared efficiently using stimulated Raman pumping, with the help of high-power narrow band nanosecond pulsed lasers. TOF spectra of the D atom products from the F + HD(v=1, j=0) reaction were measured by subtracting the TOF spectra with the Stokes laser on (F + HD(v=0 and 1, j=0)) and off (F + HD(v=0, j=0)). Figure 16 shows the experimental and theoretical 3D product contour plots for F + HD(v=1, j=0) → HF + D at collision energies of 0.23 (A and C) and 0.63 kcal/mol (B and D). The HF product was mainly produced in the v'=3 state for both collision energies, in contrast to the main HF(v'=2) products of the F + HD(v=0) reaction. The backward scattering product dominates at the collision energy of 0.23 kcal/mol, while forward scattering peaks appear at 0.63 kcal/mol. The backward scattering DCS spectrum of HF(v'=2,3) shows two broad peaks at 0.21 and 0.62 kcal/mol (Figure 17).

The dynamics calculations based on the improved FXZ-PES reproduce very well the experimentally measured DCSs (Figure 16) and the backward scattering spectrum (Figure 17). The calculated excitation function for the total angular momentum J=0,

obtained by time-dependent quantum wavepacket calculations, exhibits two distinct peaks at 0.20 and 0.66 kcal/mol, corresponding to two reactive resonance states. Analysis of the scattering wave functions for J=0 reveals the two resonance states, (204, v_1=2, v_2=0, v_3=4) and (304), at the collision energies of 0.20 and 0.66 kcal/mol respectively, where v_1 is the quantum number for the D-HF stretching mode, v_2 for the bending mode, and v_3 for the HF stretching mode. These two resonance states are the second and third excited resonance states trapped in the HF(v'=4)-D VAP well as shown in Figure 18. Further theoretical calculations indicate that the resonance mediated reaction can only be accessed via the HD(v=1) reaction pathway, while the HD(v=0) reaction path cannot access these resonances, even at high collision energies. This implies that the reagent vibrational excitation not only provides the energy required for reaction but also leads to a different reaction pathway on a distinct VAP inaccessible to the ground state reaction.

III.4.2) Short-lived Dynamical Resonances in the Cl + HD(v=1) Reaction

The Cl + H_2 reaction is also an important benchmark system in the study of chemical reaction dynamics,[98] and has been recognized as a prototypical direct abstraction reaction with a collinear reaction barrier.[99,100,101,102] No clear signature of reaction resonances has been previously observed for this reaction, although bound states in the van der Waals well of the entrance valley were characterized by SEVI of ClH_2^- and ClD_2^-.[103] In a recent study, however, Yang and coworkers detected reactive resonances in the Cl reaction with vibrationally excited HD.[68] The experiment for the Cl + HD(v=1) → DCl + H reaction is similar to that of F + HD(v=1) described above, with the HD(v=1) molecular beam prepared by stimulated Raman pumping and the Cl atom beam generated in a discharge source. Experimental measurements of the DCS at collision energies of 2.4 and 4.3 kcal/mol have been performed. Figure 19 (A and B) shows 3D product contour plots for the Cl + HD (v = 1) → DCl + H reaction. At both collision energies, the DCl products are predominantly backward scattered. However, at 4.3 kcal/mol, the experimental DCS shows a small forward scattering signal,

suggesting that a longer lived resonance state might play a role in this reaction. The collision-energy dependence of DCS in the backward scattering direction was also measured (Figure 20). This DCS exhibits two clear peaks at 2.4 kcal/mol (peak a) and 4.3 kcal/mol (peak b), suggesting that there are two resonance states in this reaction.

Theoretical calculations on a new PES reproduce the angular distribution shown in Figure 19 (C and D). Excellent agreement between theory and experiment is achieved in the backward scattering excitation function only by shifting the collision energy of the theoretical DCS lower by 0.15 kcal/mol. This small discrepancy indicates that the PES is sufficiently accurate for the dynamics. The calculated quantum dynamics reaction probability for the J=0 partial wave as a function of collision energy also shows two peaks, confirming that there may be two resonance states in this collision energy region.

Scattering wave function analyses are performed to understand the nature of these resonance states. From the nodal structures of the wavefunctions (Figure 21), two resonance states can be assigned to (v_1=1, v_2=0, v_3=2) and (122), at the collision energies of 2.4 and 4.3 kcal/mol respectively, where v_1 is the quantum number for the H-DCl stretching mode, v_2 for the bending mode, and v_3 for the DCl stretching mode. These two resonance states are transiently trapped in the H-DCl(v'=2) VAP well as shown in Figure 21. From the estimation of the widths of the resonance peaks, the lifetimes for these two resonance states are determined to be 28 and 14 fs, which are considerably shorter-lived than those in the F + HD(v=1) reaction. This is the reason that only small forward scattering signals are observed in the Cl + HD(v=1) → DCl + H reaction.

Figure 21 shows a single barrier located at the product side on the ground VAP. However, on the vibrationally excited H-DCl VAP, the interaction between H and DCl in the transition state region softens the DCl bond, manifesting in a lower vibrational frequency and, more importantly, a larger anharmonicity. The latter considerably lowers the DCl energy levels for vibrationally excited states, leading to a shallow well on the H-DCl(v'=2) VAP, which supports resonance states. The resonance-mediated

reaction mechanism is illustrated in a 1D vibrational adiabatic picture. Both resonance states can enhance the overall reactivity via shape resonance to produce DCl(v'=2), and can also decay to form DCl(v'=0, 1) via nonadiabatic couplings between VAPs. Hence, these two resonance states are also Feshbach resonances. This study has demonstrated that extremely short-lived resonances in the Cl + HD (v=1) reaction can be clearly probed with the backward scattering spectroscopy method. The discovery of the reactive resonances in the Cl + HD(v=1) reaction indicates that reactive resonances could be quite common in many chemical reactions involving vibrationally excited reagents. Hence, reactive resonances may play a significant role in the rate of reactions in important processes such as combustion, where a significant fraction of reactants are vibrationally excited due to the high temperature environment. The effects of reactive resonances on reaction rates in such processes have not yet been investigated.

III.4.3) Effects of Rotationally Excited Reactants on Resonances

The effect of a single quantum of rotational excitation of H_2 has been investigated in the F + H_2 reaction at low collision energies.[104] To study effects from the rotational excitation of H_2, two different H_2 samples were used in the experiment: normal H_2 (n-H_2) and p-H_2.[105,106] The H_2 molecules in the molecular beam are produced via supersonic expansion from a cryogenically cooled beam source, resulting in population of only the lowest rotational states: j=0 (100%) for p-H_2, and j=0 (25%) and j=1 (75%) for n-H_2. The purity of p-H_2 was measured by Raman spectroscopy of the prepared sample.[104] Using a simple calculation from the TOF signals of the H atom product measured from the F + n-H_2 and F + p-H_2 reactions, the TOF signals from the F + H_2 (j=0) and F + H_2 (j=1) reactions can be determined.

In the F + H_2 (v=0, j=0) reaction at a collision energy of 0.19 kcal/mol, the reaction products are mainly backward scattered, while a large HF(v'=2) forward scattering peak was observed in the F + H_2(j=1) reaction at the same collision energy (Figure 22). The scattering picture of the H_2(j=0) and H_2(j=1) reactions at 0.56

kcal/mol seems to be completely reversed from that at 0.19 kcal/mol, in which the reaction products are mainly backward scattered for the F + H$_2$(j=1) reaction, while a large HF(v'=2) forward scattering peak was observed in the F + H$_2$(j=0) reaction. Forward scattering of the HF (v'=2) product for the H$_2$(j=1) reaction has also been measured as a function of collision energy. A peak around 0.17 kcal/mol was observed in the excitation function, and is similar to that of F + H$_2$ (j=0),[104] except its peak is shifted to lower energy by about 0.35 kcal/mol, which is roughly equal to the rotational energy of the H$_2$ (j=1) level. Theoretical calculations suggest that the F + H$_2$ (j=1) reaction at 0.56 kcal/mol proceeds predominantly via the continuum tunneling reaction mechanism, without contribution from the two reaction resonances in the system, very different from the F + H$_2$ (j=0) reaction.[62] These experimental and theoretical results show clearly that the rotational excitation of H$_2$ only shifts the resonance energy to lower collision energy because of the addition of the rotational energy, while the resonance picture does not change in a significant way.

III. 5) Resonances in Polyatomic Reactions using Cryo-SEVI

The cryo-SEVI study of F + H$_2$ demonstrated that high-resolution transition state spectroscopy experiments can serve as benchmarks for state-of-the-art theoretical treatment of bimolecular reactive surfaces. The cryo-SEVI technique has also been applied to systems with considerably more degrees of freedom. Here we review studies of the 5-atom F + CH$_4$ → HF + CH$_3$ reaction and the 7-atom F + CH$_3$OH → HF + CH$_3$O reaction. These reactions are on the forefront of what is possible to treat theoretically, due to the difficulty of performing accurate dynamical calculations on multi-dimensional polyatomic potential energy surfaces with many degrees of freedom.

The F + CH$_4$ → HF + CH$_3$ reaction and its isotopologs have become benchmark polyatomic reactions, especially with regard to the roles that vibrational degrees of freedom and mode-selective vibrational excitation play in reaction dynamics.[107,108] F + CH$_4$ is a textbook early barrier reaction, with a low-lying transition state that

inherits much of its character from the entrance channel vdW complex. This reactant complex therefore has an emphasized role in the reaction dynamics, and the transition state spectroscopy of this region of the reactive surface is of great interest.

A schematic showing the relevant $F + CH_4$ surfaces is given in Figure 23. There are three low-lying electronic states in the entrance channel region. Working within the C_{3v} point group, the ground A_1 state is reactive (plotted with a solid curve in Figure 23), while two non-reactive E states lie nearby (dotted curves). The reactive surface has a C_{3v}-symmetric local minimum entrance channel complex where the F atom is in a linear H–C$\cdots$F arrangement. At the transition state, the C_{3v} symmetry is broken, and the F atom lies close to a single H atom, in preparation for abstraction. CH_4F^- anion has a C_{3v}-symmetric structure with a linear C-H$\cdots$F arrangement. Photodetachment from this anion structure yields good Franck-Condon overlap with both the entrance channel and transition state complexes on the neutral reactive surface.

Low-resolution overview cryo-SEVI spectra[71] are shown for detachment of both CH_4F^- and CD_4F^- in Figure 24. Photodetachment simulations calculated by Manthe and coworkers are also shown, based on full-dimensional (12D) quantum dynamics on six spin-orbit and vibronically coupled potential energy surfaces. For each isotopolog, the experimental and theoretical spectra both show two main peaks. The low-eBE peaks centered around 30,000 cm^{-1} are ascribed to transitions to the ground A_1 reactive surfaces. The higher-lying peaks centered around 31,250 cm^{-1} result from transitions to the E excited states, and are spectrally broader due to the repulsive nature of these surfaces.

High-resolution cryo-SEVI spectra of the A_1 bands of CH_4F^- and CD_4F^- are shown in Figure 25. In this narrow eBE region between 29,500 and 30,000 cm^{-1}, the spectra become highly structured. For both species, small peaks are experimentally resolved, spaced by 15-25 cm^{-1}. Similar progressions appear in the simulations. As these resonances lie below the free reactant energy asymptote, they must reside in the entrance complex vdW well. To better understand the dynamic processes that give

rise to these resonances, we turn to the results of the quantum dynamics simulations and analyze the evolution of the anion wavefunction after projection onto the neutral reactive surface. Chaotic dynamics and a high density of states prevent assignment of resonances with specific quantum numbers. However, the wavefunction motion following photodetachment is dominated by $F \cdots CH_4$ stretching and relative rotation of the fluorine and methane moieties with respect to one another, suggesting that the observed resonances stem from recurrences of these periodic motions in the entrance well. These resonances are activated owing to the difference in geometries between the anion and the entrance channel minimum-energy complex. The dense manifold of quasi-bound entrance channel states accessed here is likely to affect steering of the F + CH_4 reaction at low temperature.

As experimental and theoretical methods improve, the reaction dynamics of the more complex F + CH_3OH reaction have become a subject of recent study.[109] This hydrogen abstraction reaction can proceed barrierlessly with the fluorine atom attacking either the hydroxyl or the methyl site, leading respectively to methoxy (CH_3O) or hydroxylmethyl (CH_2OH) radical products.[110] While H-atom abstraction at the methyl group is more exothermic and statistically three times as likely as abstraction at the hydroxyl group, the hydroxyl-abstraction pathway is favored due to stabilization of its entrance complex and transition state via hydrogen bonding.

The F + CH_3OH → HF + CH_3O reaction represents a favorable case for transition state spectroscopy, with a hydrogen-bonded CH_3OHF^- anion similar in geometry to the transition state for abstraction of the hydroxyl H atom, as shown in Figure 26.[72] Interestingly, while photodetachment of the CH_4F^- anion, discussed above, predominantly accessed the entrance channel side of the transition state, photodetachment of CH_3OHF^- preferentially accesses structure in the exit channel.

Cryo-SEVI spectra of CH_3OHF^- and CH_3ODF^- are shown in Figure 27.[72] The experimental results are accompanied by a high-level simulation of the CH_3OHF^- photodetachment spectrum calculated by Guo and coworkers by running quantum dynamics trajectories on a 6-dimensional subsurface of a new 15-dimensional PES

constructed for the F + CH$_3$OH reaction. The experimental spectra are dominated by broad steps (labeled *a-e*), with an *a-b* spacing of ~3600 cm^{-1} for CH$_3$OHF$^-$ detachment and ~2700 cm^{-1} for CH$_3$ODF$^-$. Previous photodetachment experiments[111,112] also observed this stepped structure and assigned it to an H−F stretching progression of the CH$_3$O−HF product complex (PC). The location of the structure with respect to the product and reactant asymptotes confirms that indeed, the observed structure can only lie in the PC well. The states in feature *a* lie below the product asymptote and are therefore bound with respect to free products, while features *b-e* are metastable and will eventually dissociate via vibrational predissociation as vibrational energy flows to translational motion along the reaction coordinate. As all resonances seen here lie below the reactant asymptote, they are inaccessible to F + CH$_3$O scattering experiments and therefore uniquely accessible with an anion photodetachment scheme.

With cryo-SEVI, additional fine structure is newly resolved, superimposed on the broad steps and spaced by ~200 cm^{-1}. This fine structure is well-reproduced by the simulation, including the subtlety that the spacing of resonances within each step increases with increasing eBE (*e.g.* peaks *a1-a2* are more finely spaced than peaks *b1-b2*, which are more finely spaced than peaks *c1-c2*). The nature of this fine structure can be explained with reference to the VAPs sketched in Figure 26, which correlate to free HF(*v*) + CH$_3$O products. The spectral steps *a-e* each represent detachment to an HF(*v*=0-4) VAP, while the fine peaks within each step are resonances supported in the VAP wells with excitation in the CH$_3$O−HF vdW stretching mode. VAP wells are known to deepen with increasing vibrational excitation, through dynamical vibrational bonding.[113] In this case, the VAP wells are stabilized as the HF stretching excitation is increased and the H atom becomes more delocalized between the heavier F and CH$_3$O fragments. This gives rise to the observed increase in CH$_3$O−HF level spacing with increasing eBE.

These vibrational assignments can be confirmed with reference to vibrational wavefunctions extracted from the photodetachment simulations. Wavefunctions

corresponding to several relevant spectral peaks are plotted in Figure 28. Based on the localization of these states, it is again clear that they are bound or quasi-bound resonances supported in the product well; the quasi-bound states are vibrational Feshbach resonances that can dissociate to products.   Considering the nodal structure of the plotted wavefunctions, each subsequent spectral hump (e.g. the *a1-b1-c1* progression) shows an increasing integer number of nodes along the HF stretching coordinate (vertical axis). These broad humps do therefore correspond to increasing excitation of the product complex HF stretching vibration. Within each hump (e.g. the *a1-a2-a3* progression), the narrow spectral features show increasing nodes along the CH_3O-HF coordinate (horizontal axis), confirming the assignment of the fine vibrational structure to excitation of the stretching mode between the two product complex fragments. The increased intensity of the higher-eBE peaks is also explained by these vibrational wavefunctions: for instance, *d1* has considerably better FC overlap with the CH_3OHF^- anion wavefunction than *a1* does.

Taken together, the $F + CH_4$ and $F + CH_3OH$ studies illustrate the utility and clarity of cryo-SEVI spectroscopy for probing detailed dynamical resonances in the transition state regions of increasingly intricate bimolecular reactions. These studies permit benchmarking of state-of-the-art quantum dynamics calculations, which have only recently become capable of treating multidimensional systems of this size and complexity.

IV.   Concluding Remarks

As illustrated by this overview of recent advances in the study of reactive resonances in a few benchmark reactions, the combination of improved experimental methods and highly accurate quantum dynamics calculations has yielded a detailed understanding of the nature of these resonances and how they affect reaction dynamics. Using high-resolution anion photoelectron spectroscopy, resonance states lying to either side or directly on top of the reaction barrier can be detected, yielding a

clearer picture of the entire transition state region. However, not all quantized states in the transition state region have a significant effect on the reaction dynamics. High-resolution crossed beam backward scattering spectroscopy has proved to be a very powerful tool to understand which resonances affect reactivity , by directly measuring the collision energies that access reaction resonance states, the lifetime of these resonances, and the resulting product states formed. The examples provided in this review have demonstrated that slow photoelectron velocity-map imaging of cryo-cooled anions and crossed beam backward scattering spectroscopy provide complementary insights and allow one to understand reactive resonances at an unprecedented level.

This review article has focused mainly on recent progress made in the study of reactive resonances in two benchmark systems: $F + H_2$ (HD, D_2) and $Cl + HD$. In addition to these systems, resonance phenomenon in other reactions have been investigated. In the $S(^1D_2) + HD \rightarrow SH + D$ reaction, three resonances at very low collision energy have been observed by Costes and coworkers,[114,115] however, quantum dynamics theory has not been able to identify and assign these resonances.

Now that the existence of resonances has been confirmed for a number of benchmark reactions, it is of considerable interest to determine how widespread resonance are and to develop new experimental and theoretical methods to characterize them. For example, using backward scattering spectroscopy, it may be possible to observe resonances for polyatomic reactions in scattering experiments. The new field of cold molecule chemistry enables the study of chemical reactions at extremely low temperatures.[116,117] Such experiments are likely to be very senstitive to the presence of reactive resonances, since quantum mechanical tunneling and related effects will play an outsize role in the measured cross sections and rate constants.[118]

Acknowledgements

Figures and Captions
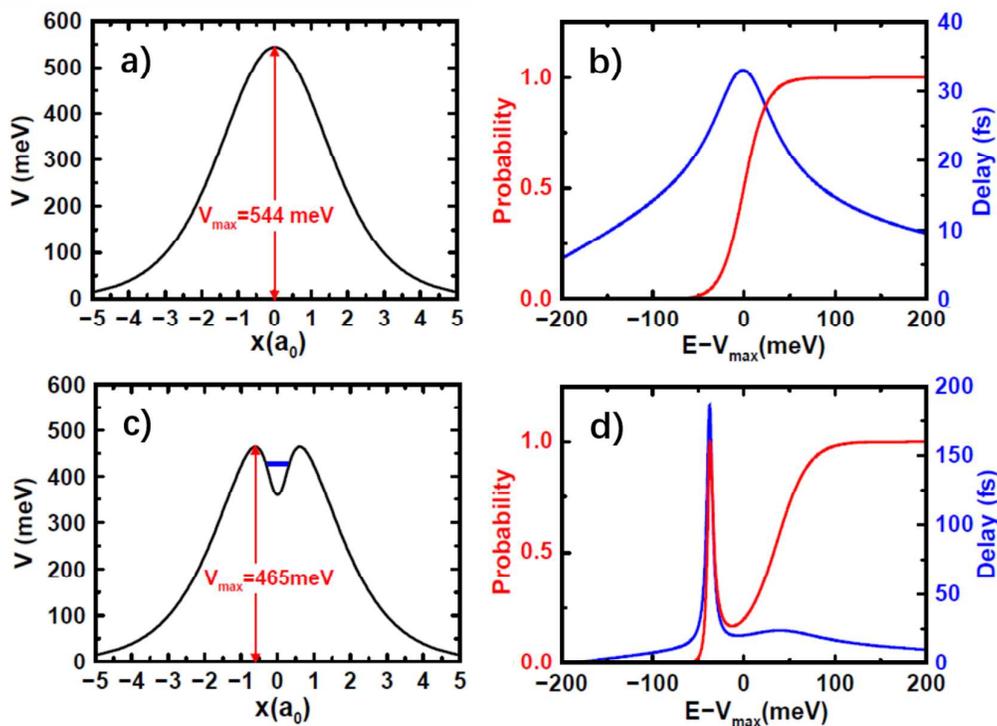
Figure 1. Two one-dimensional model reactions: one with a simple barrier and the other with a reactive resonance: (a) the potential energy curve along the reaction coordinate for a model reaction with a simple barrier; (b) the calculated reaction probability (red curve) and time delay (blue curve) for the model reaction in panel a; (c) the potential energy curve along the reaction coordinate for a model reaction with a dynamical resonance; (d) the calculated reaction probability (red curve) and time delay (blue curve) for the model reaction in panel c. Reproduced from ref. 15 with permission from the Elsevier, copyright 1991.
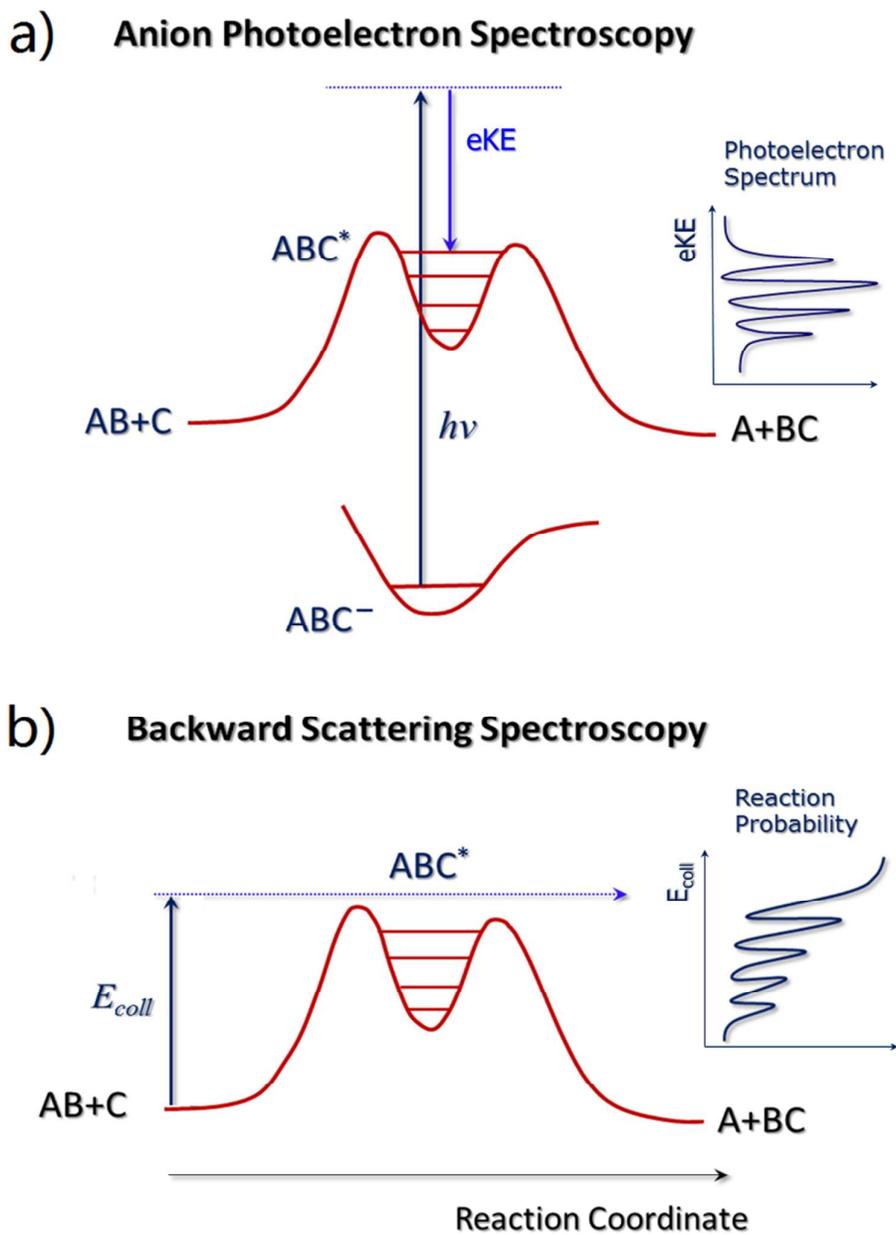
Figure 2. Schematics of the two transition state spectroscopy methods: anion photoelectron spectroscopy and crossed moleecular beam backward scattering spectroscopy.
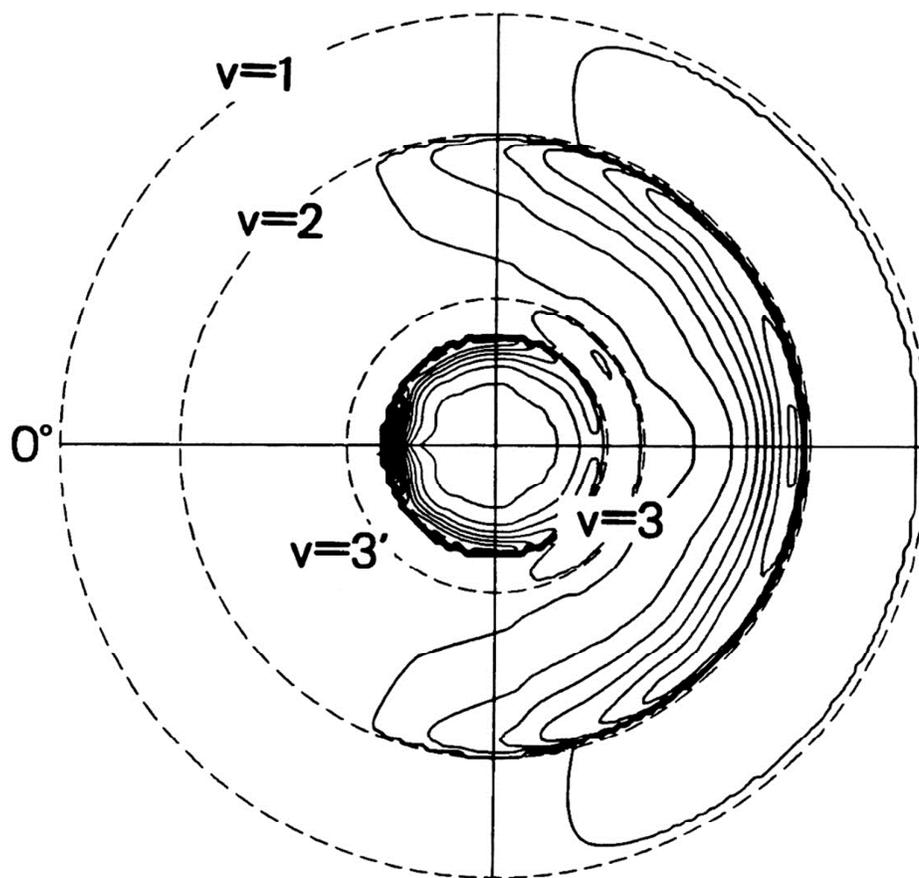
Figure 3. The center-of-mass flux-velocity contour map for the F+*p*-H$_2$ reaction at the collision energy of 1.84 kcal/mol. Note the pronounced forward scattering (0° degree) peak for *v*=3. Reproduced from ref. 51 with permission from the American Institute of Physics, copyright 1985.
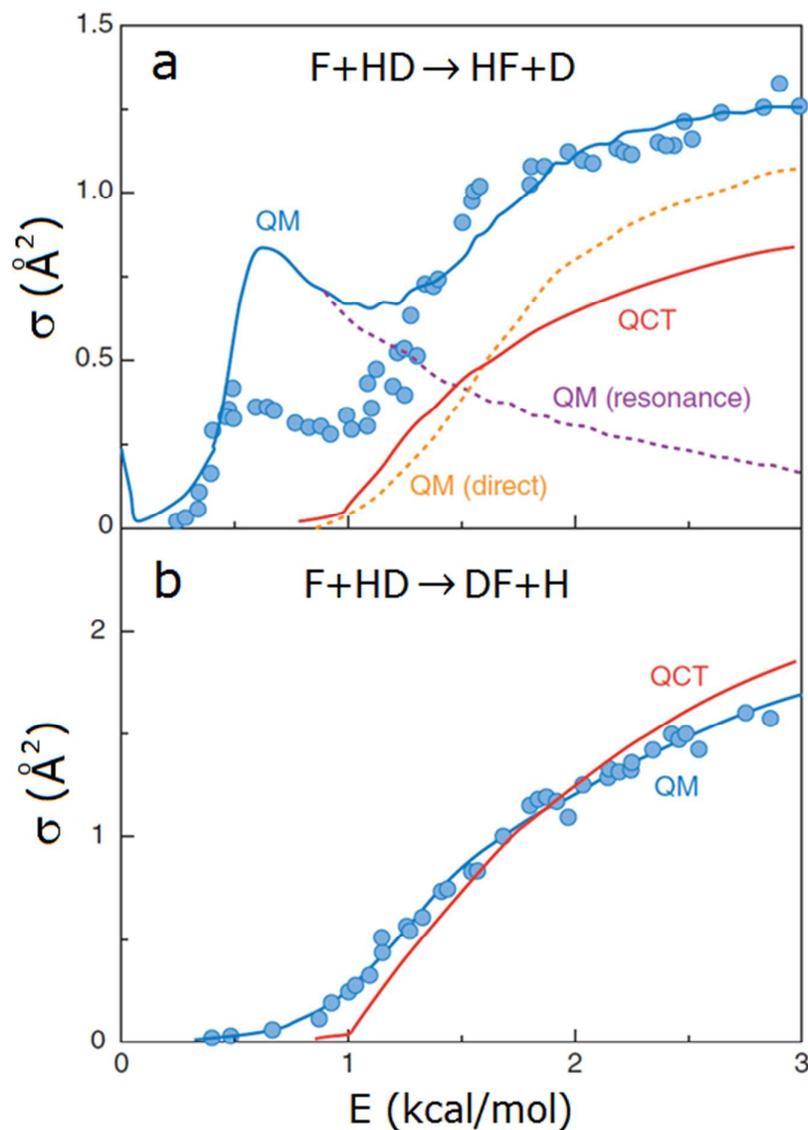
Figure 4. The excitation functions, or integral cross sections as a function of collision energy, of the two isotopic product channels in the F + HD reaction. The experimental results (solid dots) are normalized to QCT and QM theoretical results by a single scaling factor for both channels. Reproduced from ref. 60 with permission from the American Institute of Physics, copyright 2000.
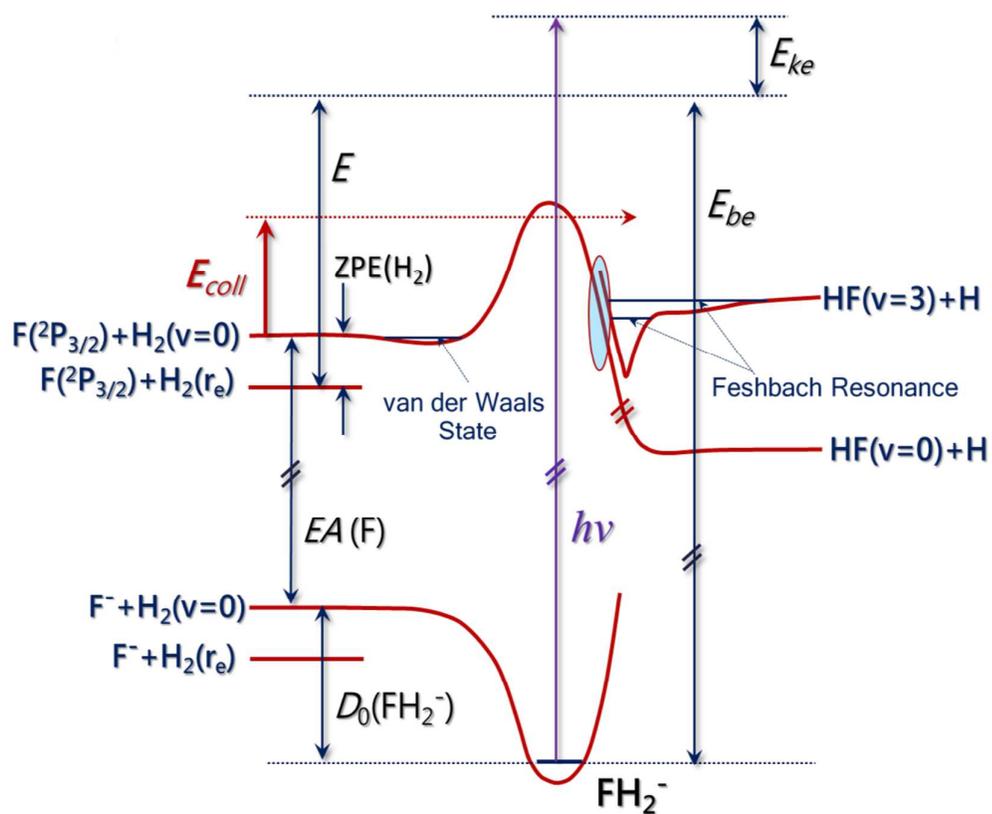
Figure 5. Schematic energy diagram of the photodetachment process from the FH_2^- to the $F + H_2$ reactive surface.
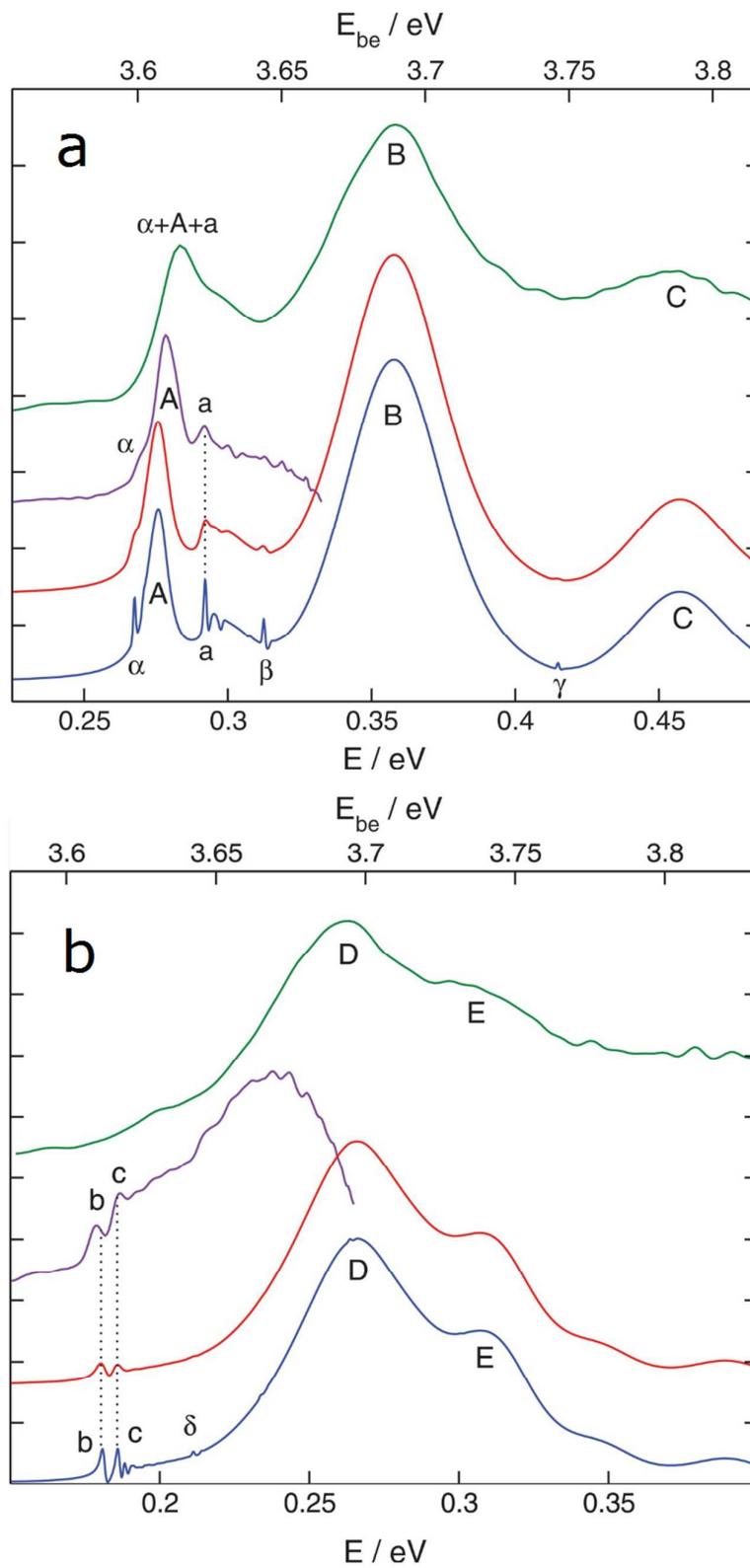
Figure 6. Photodetachment spectra of (a) *p*-FH$_2$$^-$ and (b) *n*-FD$_2$$^-$. The experimental overview spectra (~10 meV resolution) are shown in green, while the highest

resolution (2 to 3 meV) experimental cryo-SEVI spectra taken over narrower energy windows are shown in purple. Theoretical simulations are shown at 1 meV energy resolution (blue) and 3 meV resolution (red). The calculated spectra have not been shifted to match experiment. For $p\text{-FH}_2^-$, the relation between the experimental electron binding energy E_{be} and the energy E relative to $F(^2P_{3/2}) + H_2(r_e)$ is given by $E_{be} = E + 3.3312$ eV. Reproduced from ref. 70 with permission from the AAAS, copyright 2015.
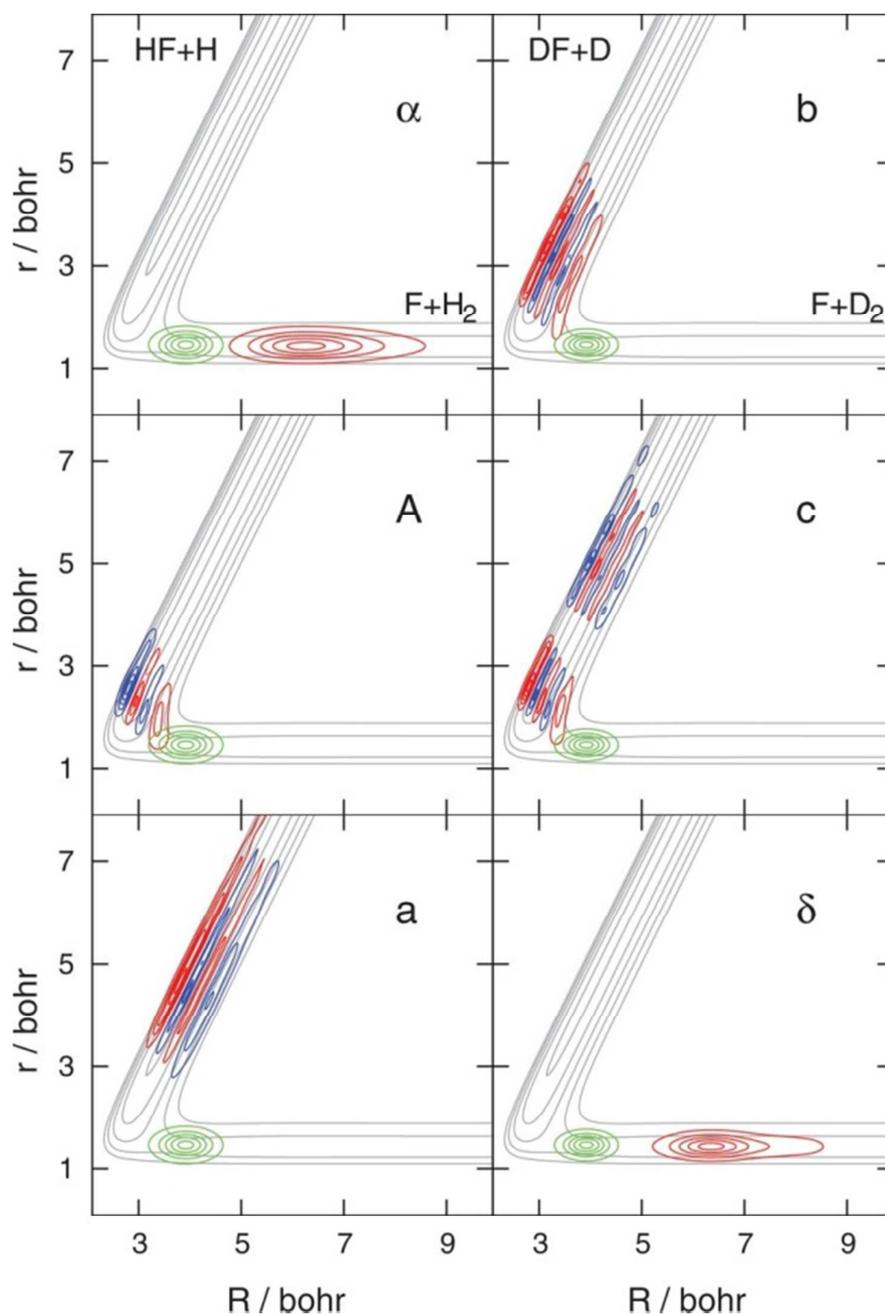
Figure 7. Wavefunctions at the energies of the first three peaks in the theoretical p-FH$_2^-$ spectrum (α, A, a; left) and n-FD$_2^-$ spectrum (b, c, δ; right) from Figure 2. The wavefunctions are plotted in red and blue contours, superimposed on the contours of the LWAL potential energy surface (gray), as a function of R, the distance between F and the center-of-mass of H$_2$/D$_2$, and r, the bond length of H$_2$/D$_2$. The FH$_2^-$ and FD$_2^-$ anion wavefunction contours are shown in green. Reproduced from ref. 70 with permission from the AAAS, copyright 2015.
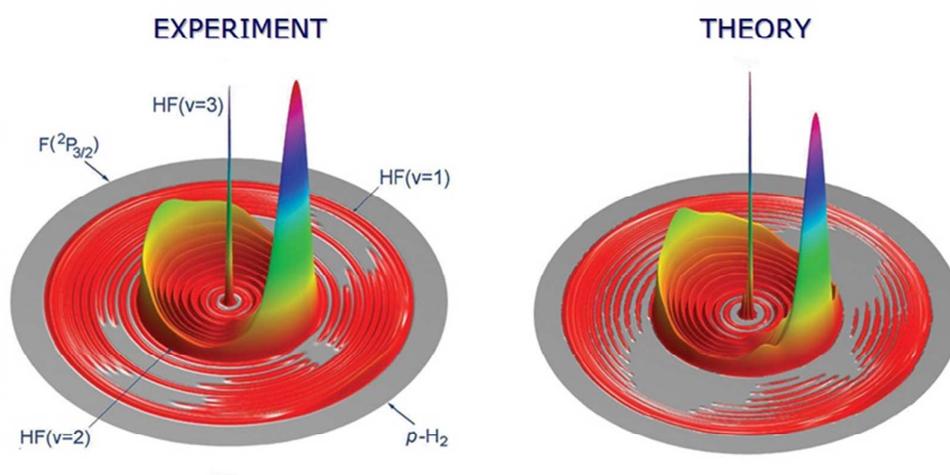
Figure 8. Experimental and theoretical three-dimensional contour plots for the HF product translational energy and anglular distributions of the $F+H_2(j=0)$ reaction at a 0.52 kcal/mol collision energy. Different rings represent different HF product rovibrational states. Reproduced from ref. 62 with permission from the AAAS, copyright 2006.
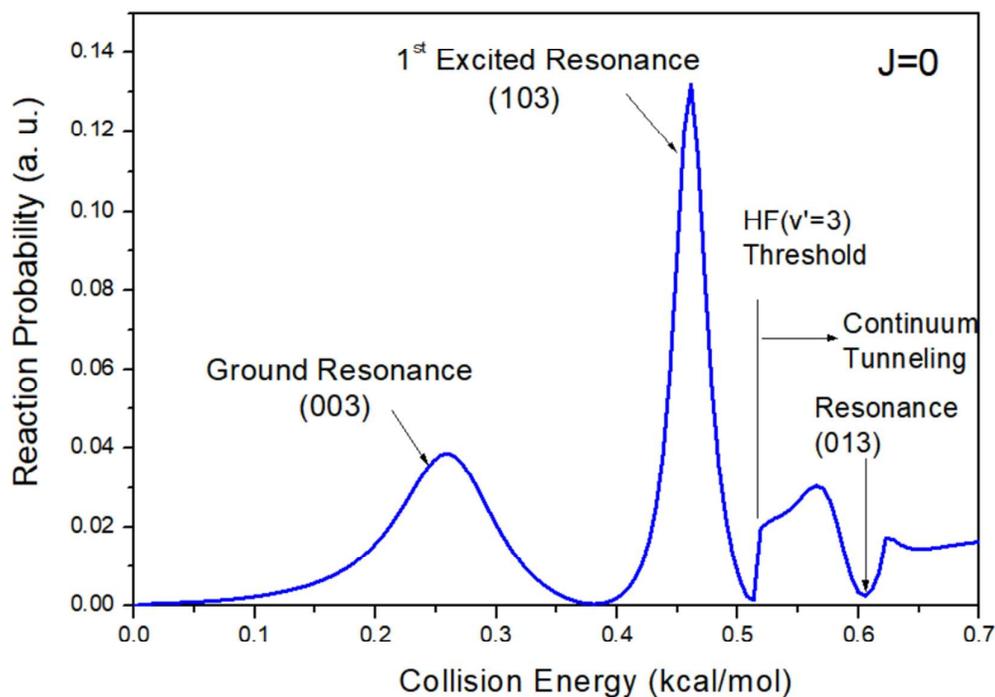
Figure 9. J=0 reaction probability for the HF(v'=2) product of the F+H$_2$ (j=0) reaction. Reproduced from ref. 62 with permission from the AAAS, copyright 2006.
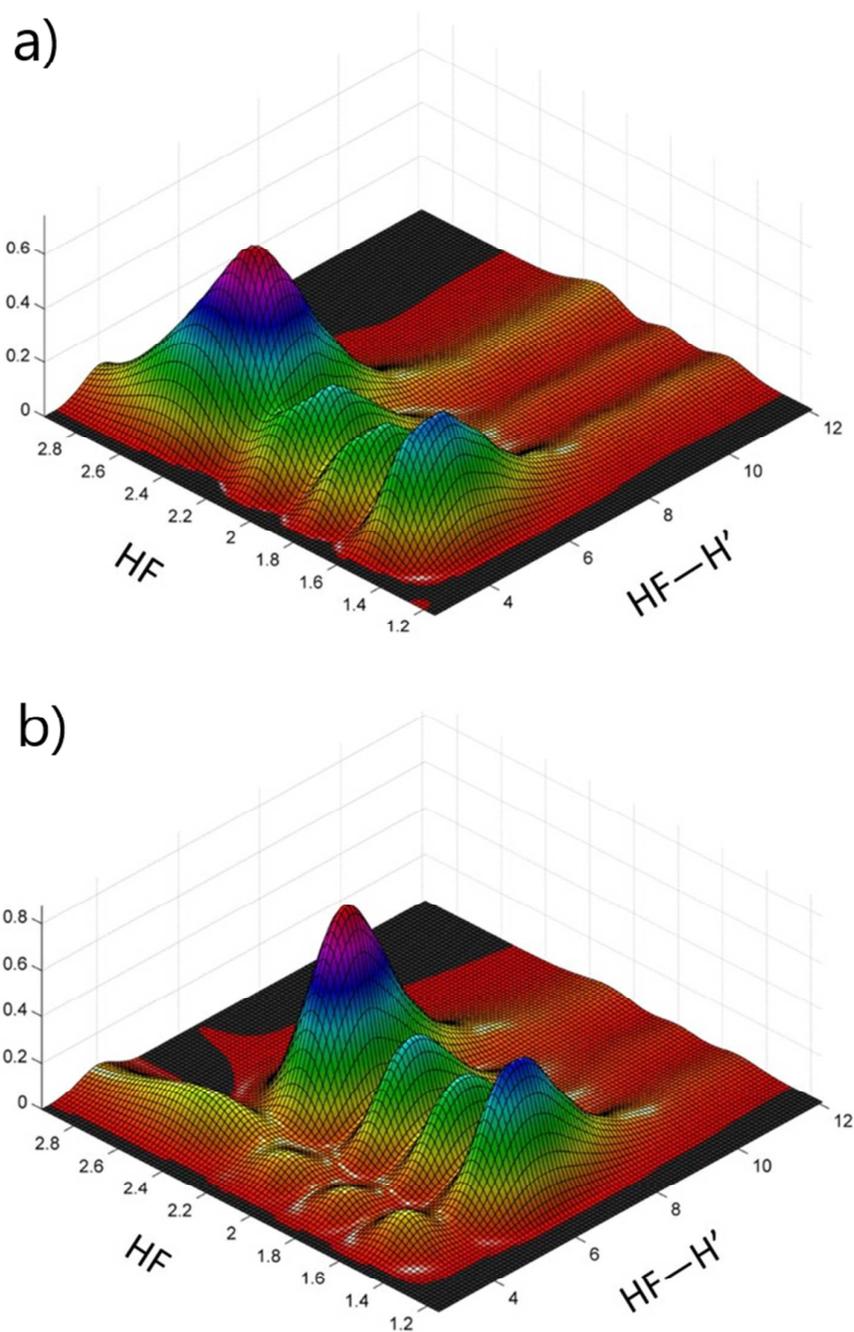
Figure 10. 3D scattering wave functions for the F + H$_2$ reaction with *J*=0 at (a) 0.26 and (b) 0.46 kcal/mol collision energies. Reproduced from ref. 62 with permission from the AAAS, copyright 2006.
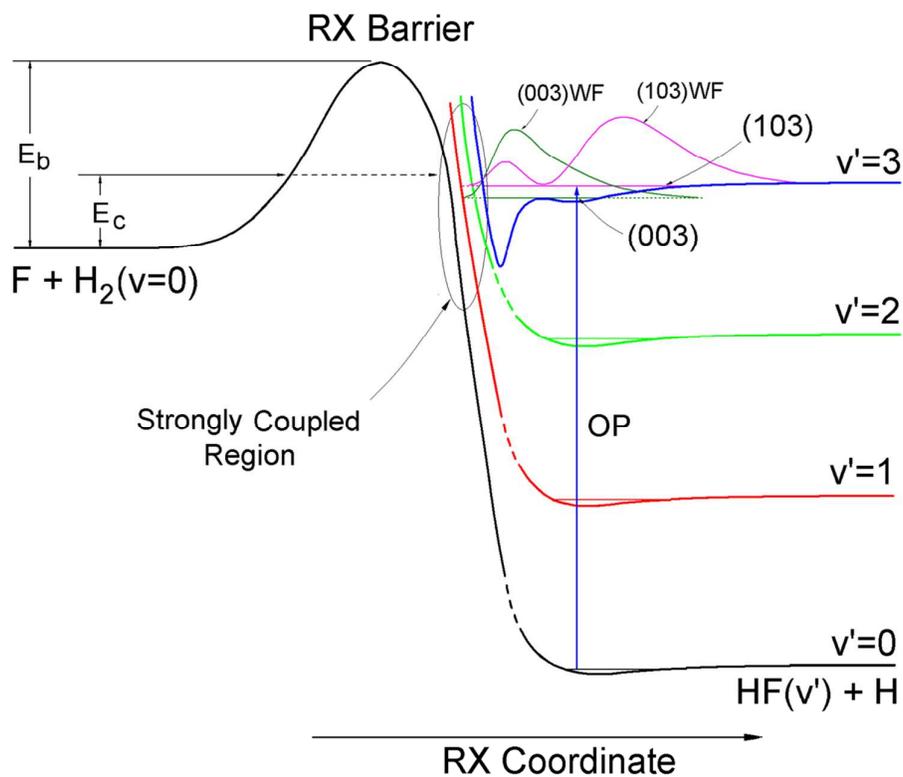
Figure 11. Schematic diagram showing the resonance-mediated reaction mechanism for the F + H$_2$ reaction with two resonance states trapped in the peculiar HF(v'=3)-H' vibrational adiabatic potential well along the reaction (RX) coordinate. The 1D wave functions of the two resonance states are also shown. Reproduced from ref. 62 with permission from the AAAS, copyright 2006.
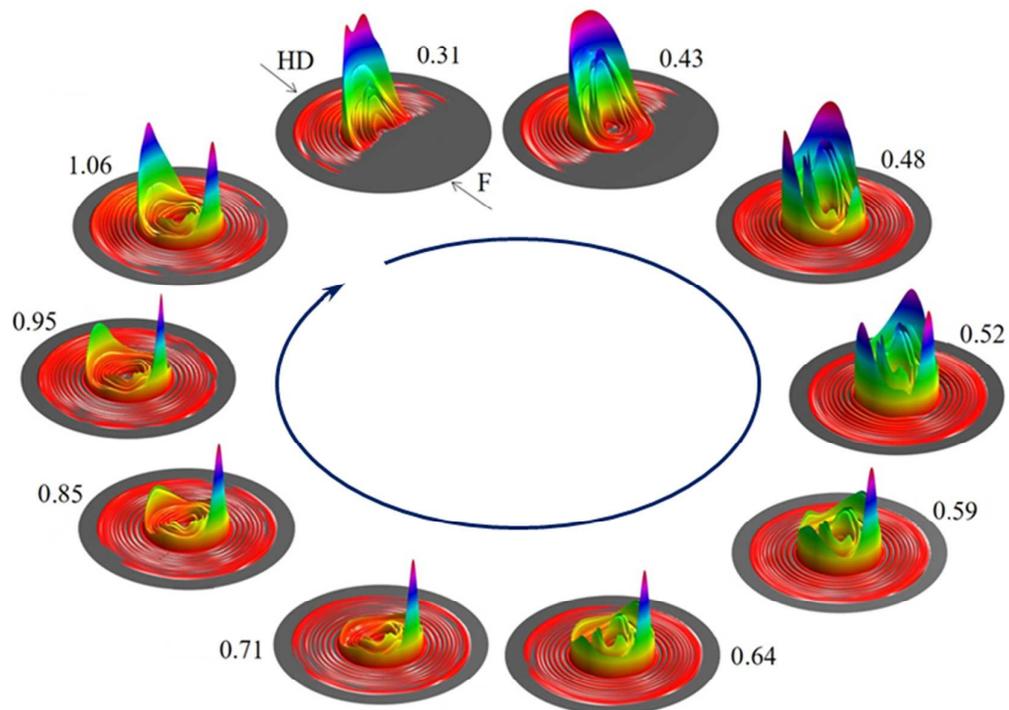
Figure 12. Experimental three dimensional D-atom product flux contour plots for the F + HD(j=0) → HF(v',j') + D reaction at different collision energies from 0.31 to 1.06 kcal/mol. Reproduced from ref. 64 with permission from the National Academy of Sciences, copyright 2008.
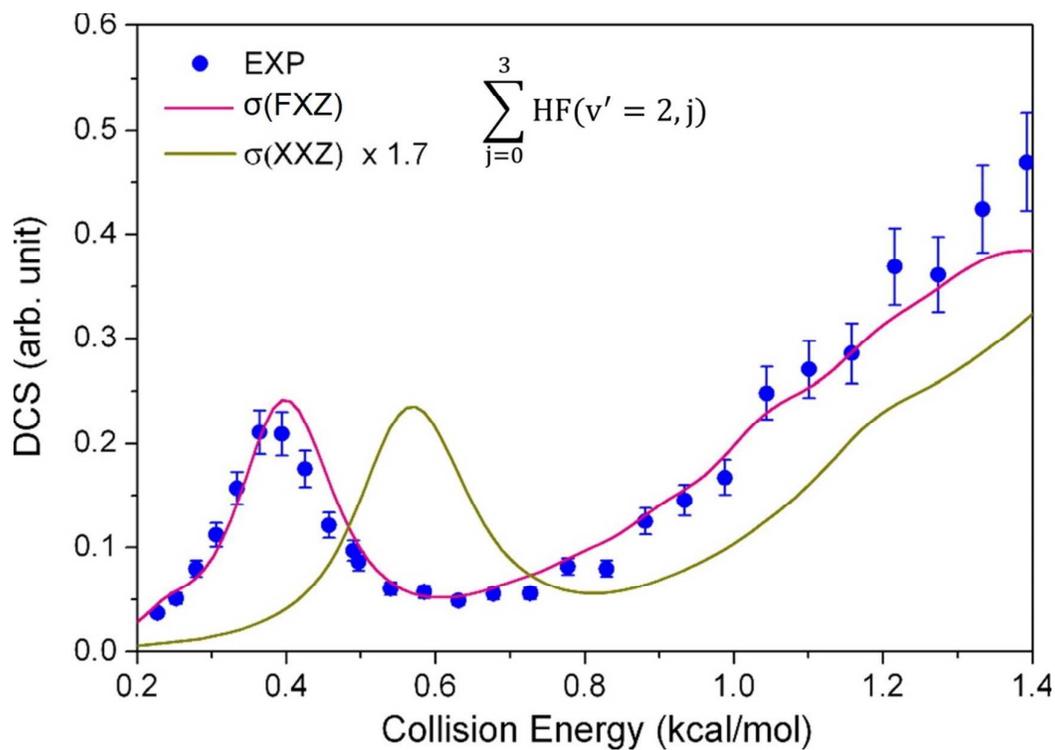
Figure 13. Collision energy-dependent DCS for the backward scattering HF(v'=2) products summed over j'=0, 1, 2 and 3. The solid circles are the experimental data, and the solid lines are the calculated theoretical results based on the XXZ- and FXZ-PES. Reproduced from ref. 64 with permission from the National Academy of Sciences, copyright 2008.
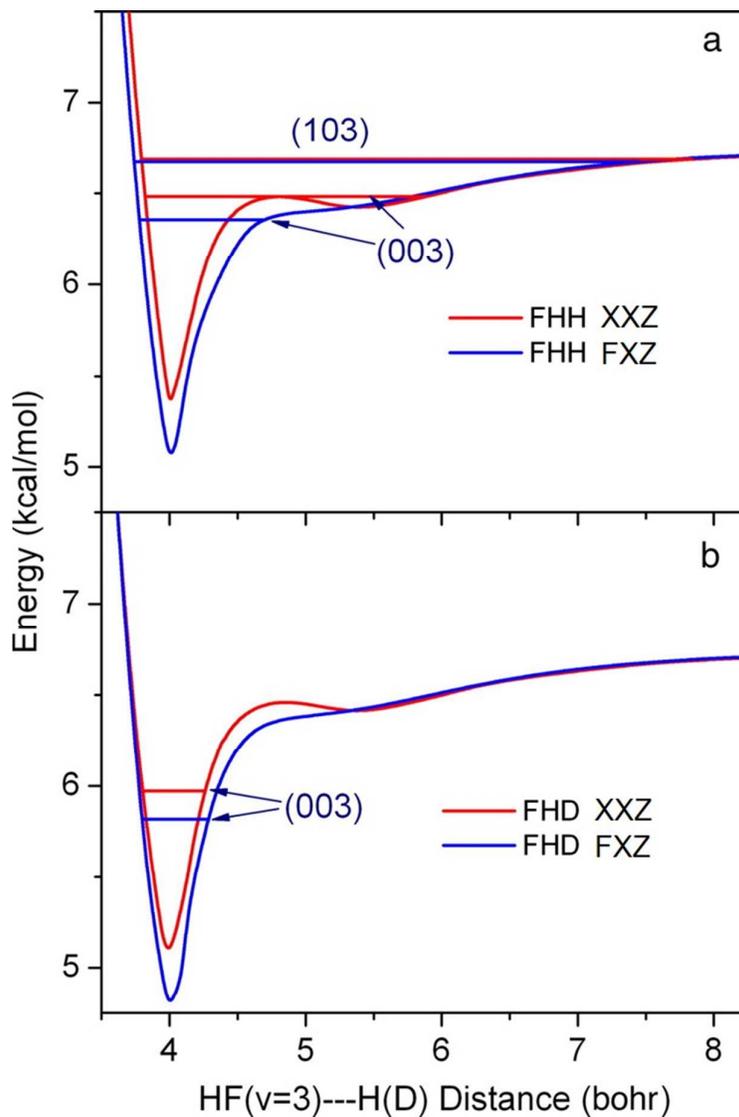
Figure 14. (a) The one-dimensional adiabatic resonance potentials of (a) HF(v=3)-H for the F + H$_2$ reaction and (b) HF(v'=3)-D for the F + HD reaction traced out from the XXZ-PES and the FXZ-PES. Reproduced from ref. 64 with permission from the National Academy of Sciences, copyright 2008.
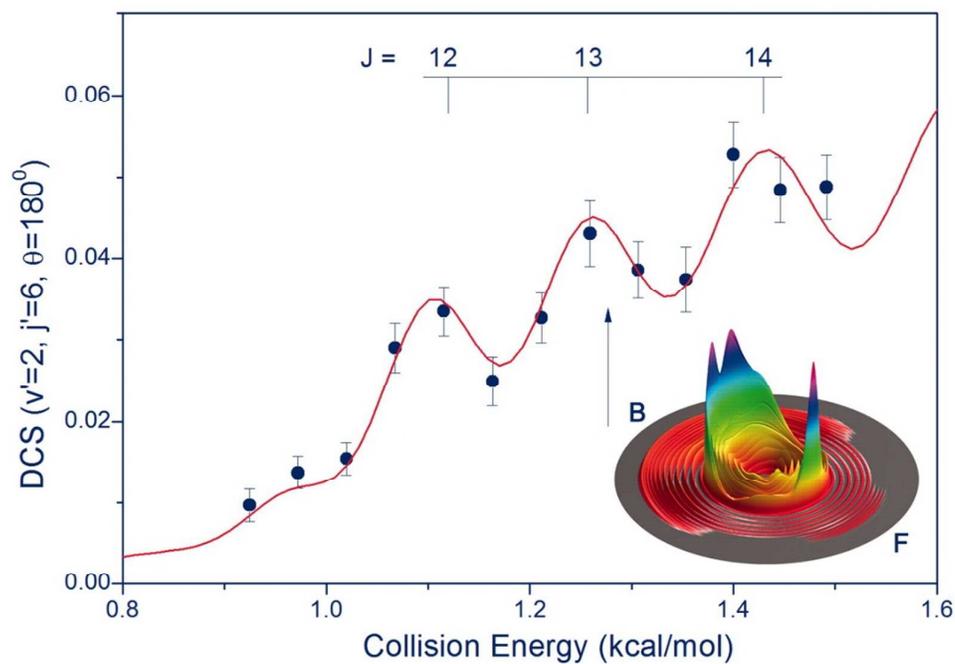
Figure 15. Experimental (solid circles) and theoretical (red curve) DCS of the HF(v'=2, j'=6) product of the F + HD(j=0) reaction in the backward scattering direction. The theoretical result was convoluted with the experimental resolution and shifted 0.03 kcal/mol lower in energy. The inset 3D DCS shown was measured at 1.285 kcal/mol. Reproduced from ref. 89 with permission from the AAAS, copyright 2010.
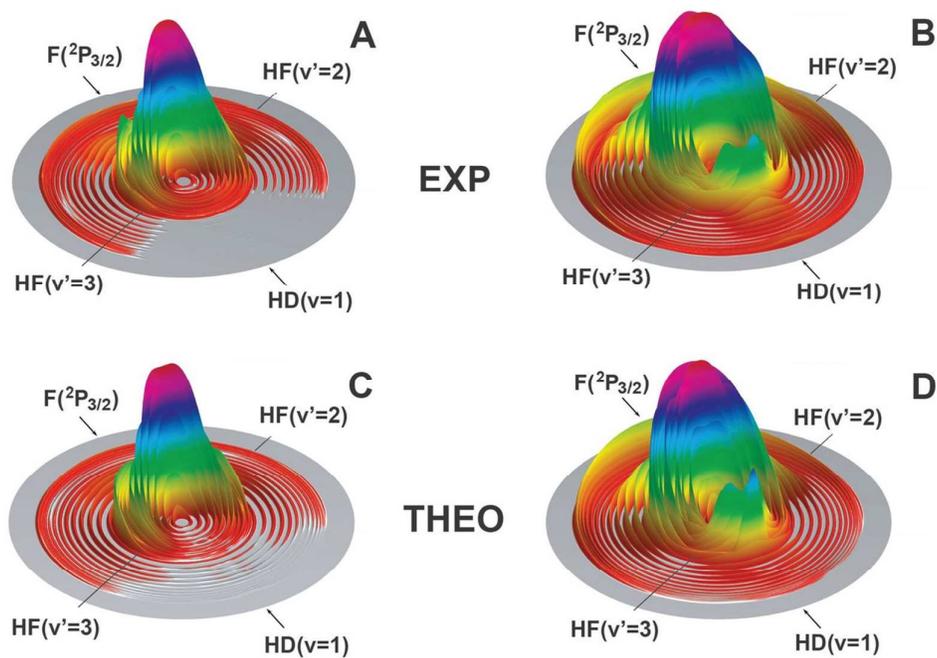
Figure 16. The experimental and theoretical 3D product contour plots for the F + HD(v=1, j=0) $\rightarrow$ HF + D reaction at collision energies of 0.23 (A and C) and 0.63 kcal/mol (B and D). Reproduced from ref. 67 with permission from the AAAS, copyright 2013.
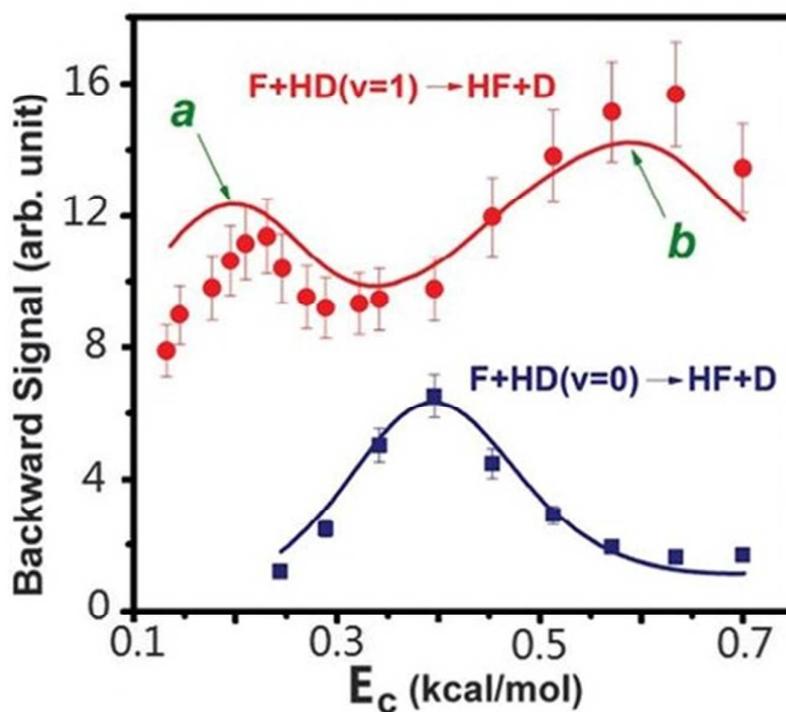
Figure 17. Experimental (solid circles and squares) and theoretical (solid lines) DCS for the backward scattered HF products of the F + HD ($v = 1$, $j = 0$) reaction (red line and circles) and the F + HD reaction ($v = 0$, $j = 0$) (blue line and squares), over a range of collision energies E_c. Reproduced from ref. 67 with permission from the AAAS, copyright 2013.
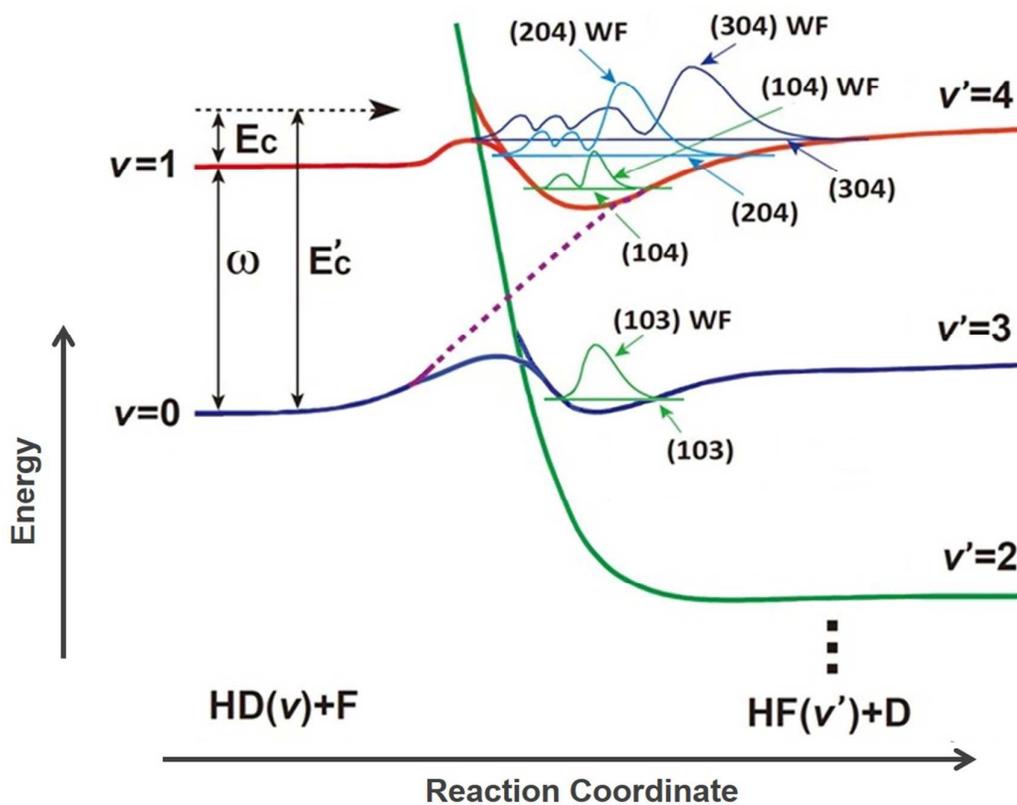
Figure 18. Schematic diagram showing the resonance-mediated reaction mechanism for the F + HD → HF + D reaction. Three resonance states, (104), (204), and (304), are trapped in the HF ($v' = 4$)–D VAP well. Only the HD(v=1) reactant can effectively correlate with the (204) and (304) resonance states. Reproduced from ref. 67 with permission from the AAAS, copyright 2013.
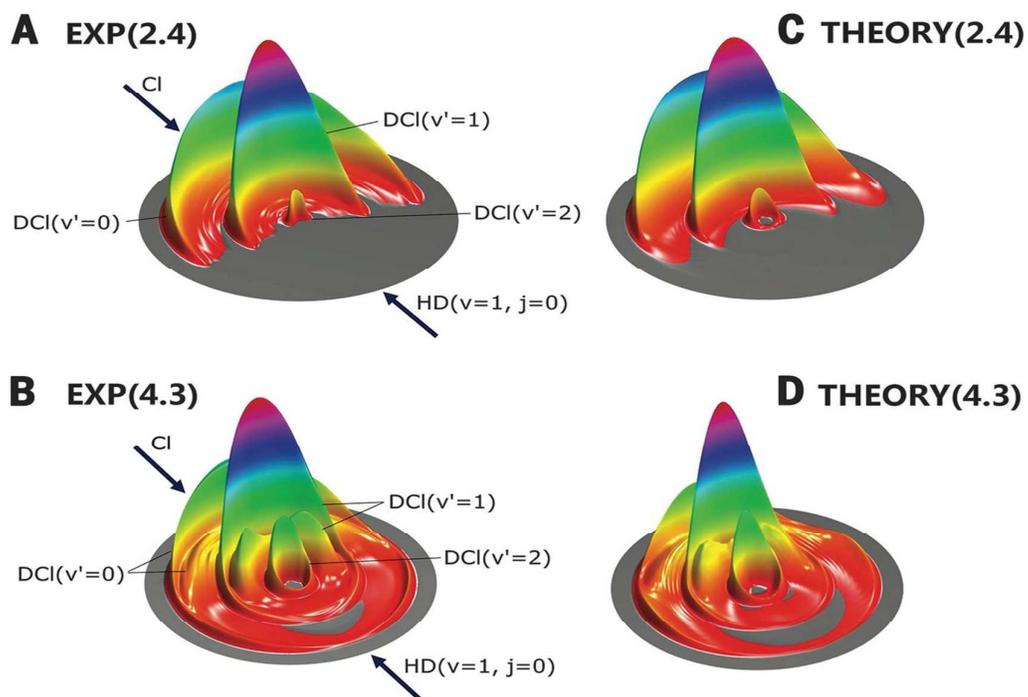
Figure 19. 3D scattering product contour plots as a function of product velocity for the Cl + HD ($v = 1$) → DCl + H reaction. The experimental (A and B) and theoretical (C and D) results are shown at collision energies of 2.4 (A and C) and 4.3 kcal/mol (B and D). Reproduced from ref. 68 with permission from the AAAS, copyright 2015.
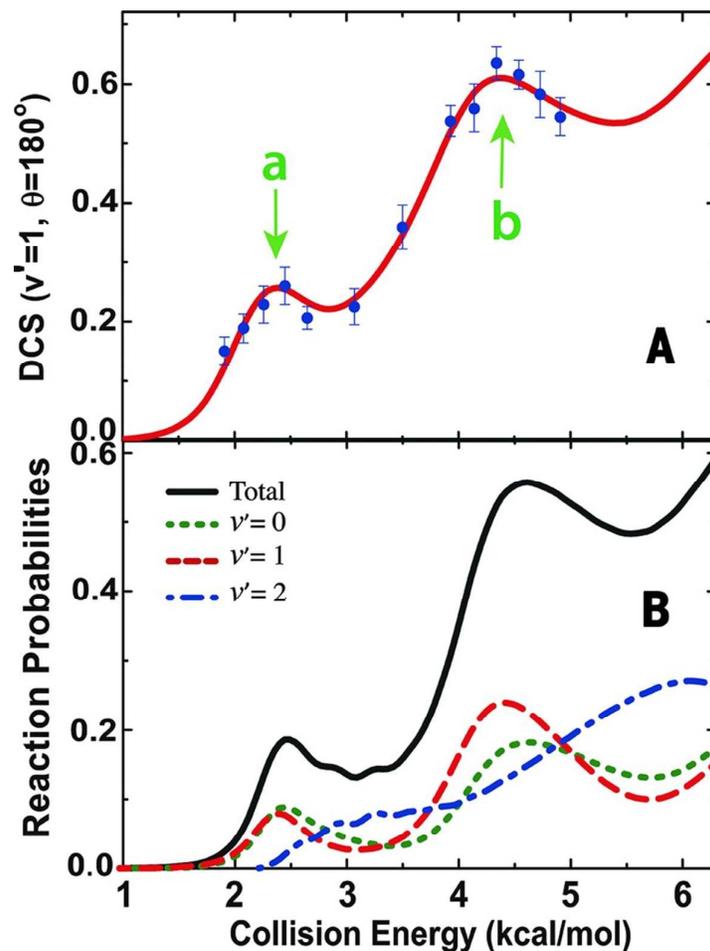
Figure 20. (A) Theoretical (solid red lines) and experimental (solid circles) DCS for the backward scattered DCl product of Cl + HD ($v = 1, j = 0$) over a range of collision energies. The theoretical DCS was shifted 0.15 kcal/mol lower in energy for the comparison. (B) Total and product state-resolved reaction probabilities with $J = 0$ as a function of collision energy. Reproduced from ref. 68 with permission from the AAAS, copyright 2015.
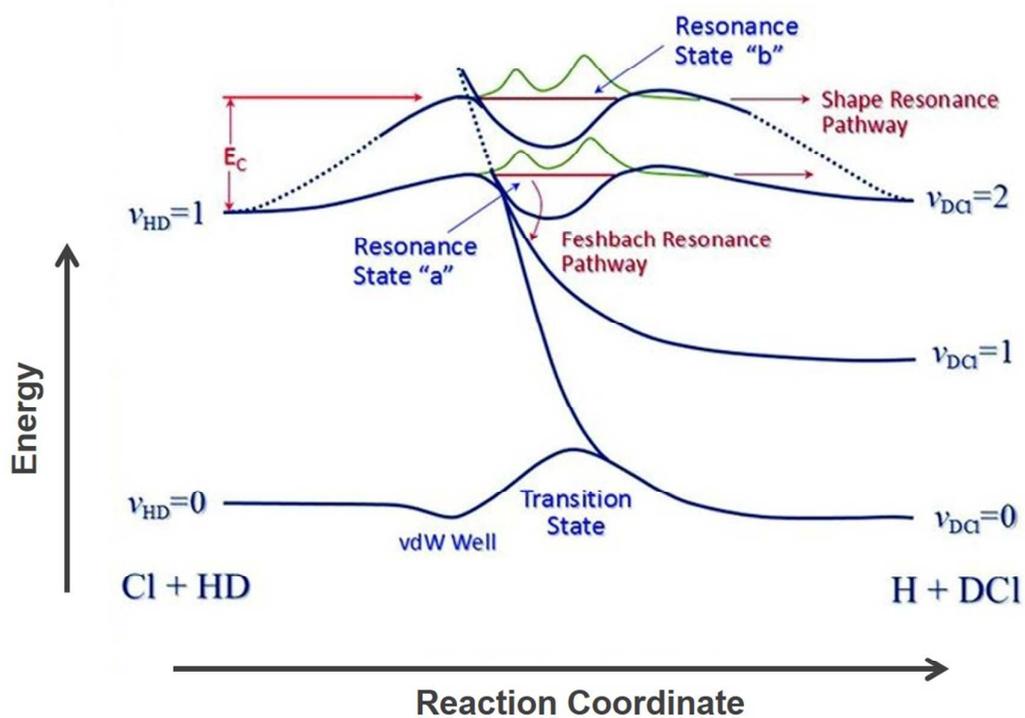
Figure 21. VAPs along the reaction coordinate for the Cl + HD reaction. The VAPs of $v_{HD}=1$ and $v_{DCl}=2$ are strongly correlated, and because of chemical bond softening in the transition state region, resonance states above the $v_{DCl}=2$ VAP well are produced. Reproduced from ref. 68 with permission from the AAAS, copyright 2015.

0.19 kcal/mol

0.56 kcal/mol

a) j=0
v=2
B
v=1
F

b) j=0
B
v=2
v=1
F

c) j=1

d) j=1
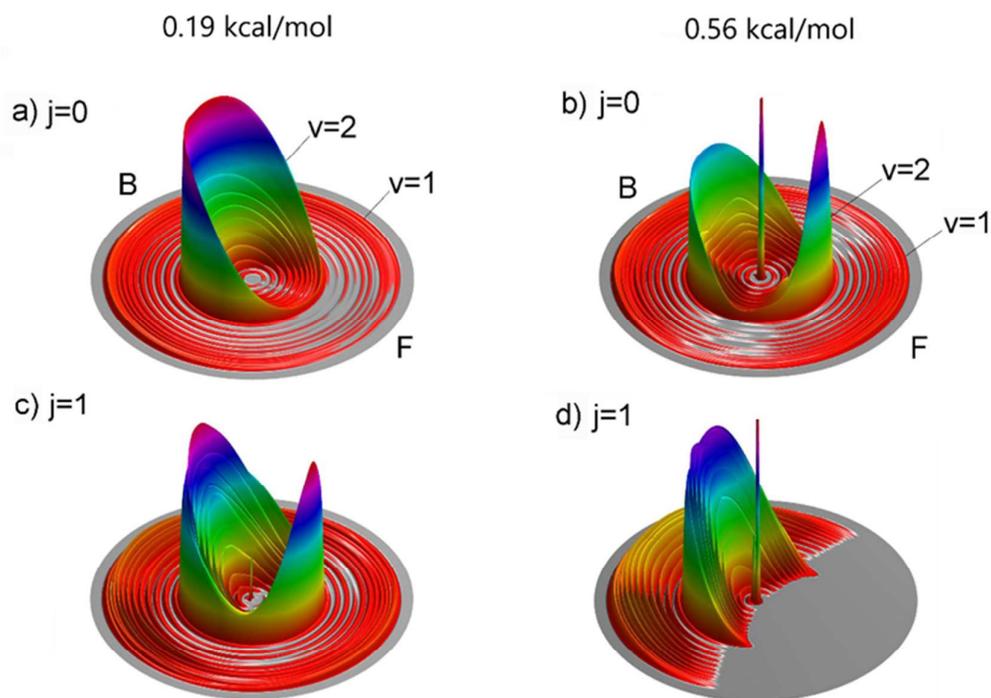
Figure 22. Three dimensional plots of the experimental differential cross sections for the F + H$_2$(j=0,1)→HF + H reaction at collision energies of 0.19 and 0.56 kcal/mol. Reproduced from ref. 104 with permission from the American Institute of Physics, copyright 2006.
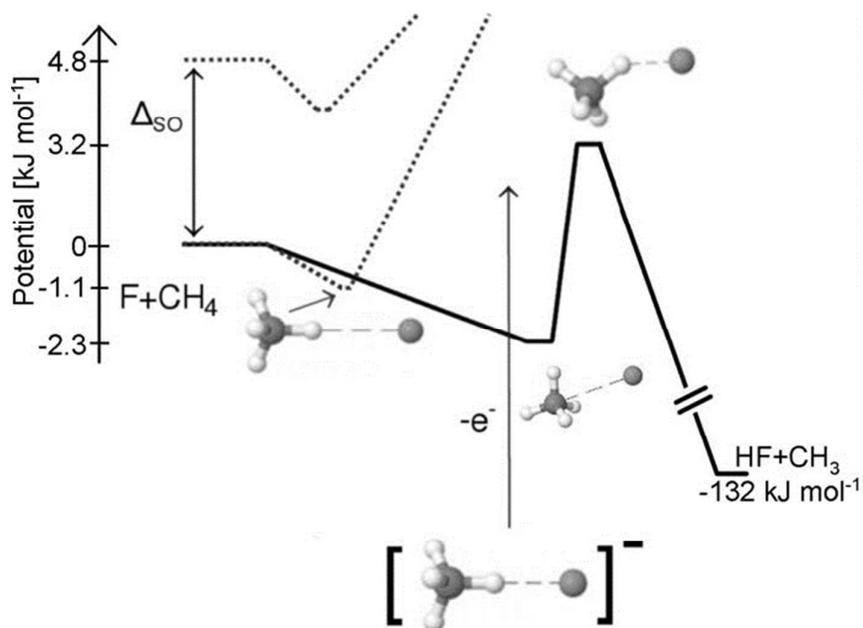
Figure 23. Schematic of relevant PESs involved in the $F + CH_4 \rightarrow HF + CH_3$ reaction, accessed through photodetachment of the CH_4F^- anion complex (indicated with a vertical arrow). The reactive A_1 surface is shown with a solid curve, while the dotted curves represent the non-reactive E surfaces. Δ_{SO} represents the spin-orbit splitting of atomic F. Reproduced from ref. 71 with permission from the Wiley-VCH, copyright 2014.
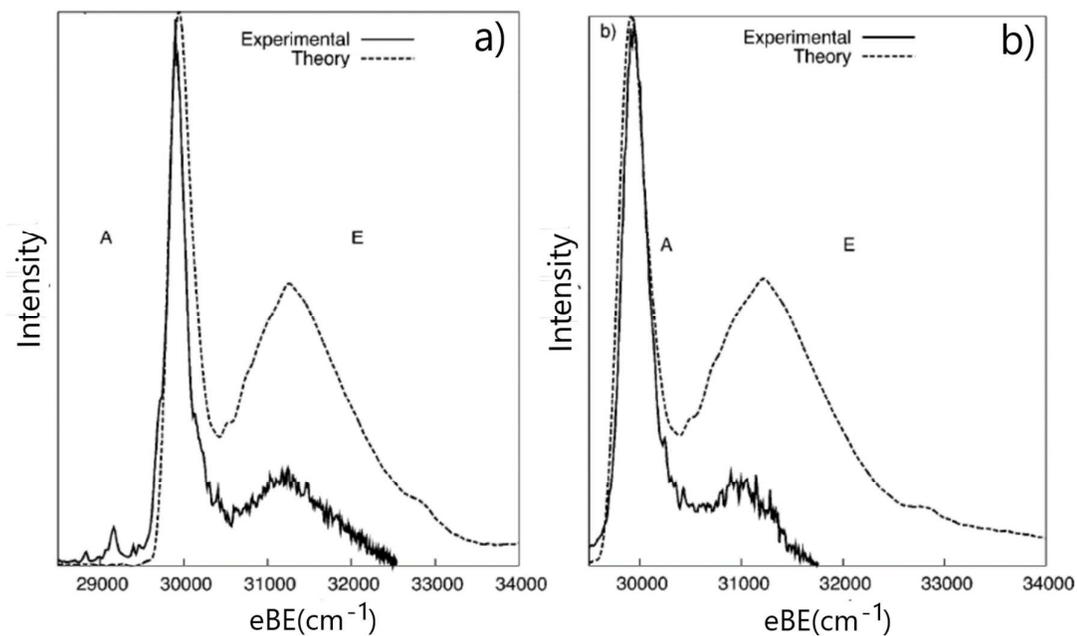
Figure 24. Low-resolution overview cryo-SEVI spectra for a) CH_4F^- and b) CD_4F^- photodetachment (solid lines), compared to theoretical simulations (dotted lines). Reproduced from ref. 71 with permission from the Wiley-VCH, copyright 2014.
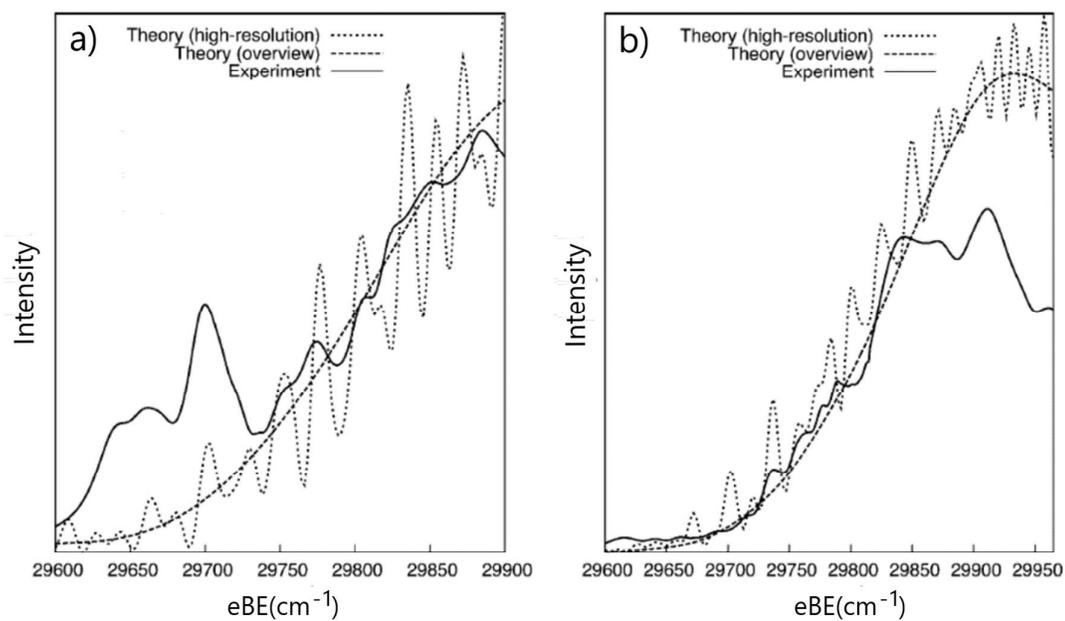
Figure 25. High-resolution cryo-SEVI spectra for a) CH_4F^- and b) CD_4F^- photodetachment (solid lines), compared to high- and low-resolution theoretical simulations (dotted lines). Reproduced from ref. 71 with permission from the Wiley-VCH, copyright 2014.
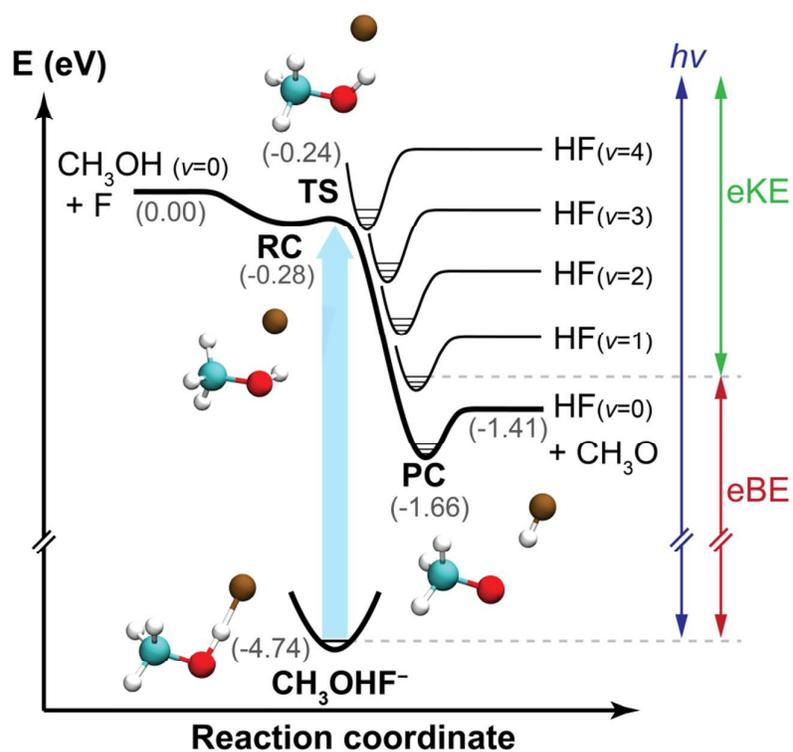
Figure 26. Schematic energy diagram for photodetachment of the CH_3OHF^- anion to the neutral $F + CH_3OH \rightarrow HF + CH_3O$ reactive surface. The bold line is the zero-point energy corrected surface connecting reactants and products in their ground vibrational states. Calculated geometries and energies are shown for the anion, reactant complex (RC), transition state (TS) and product complex (PC) stationary points. Reproduced from ref. 72 with permission from the Springer Nature, copyright 2017.
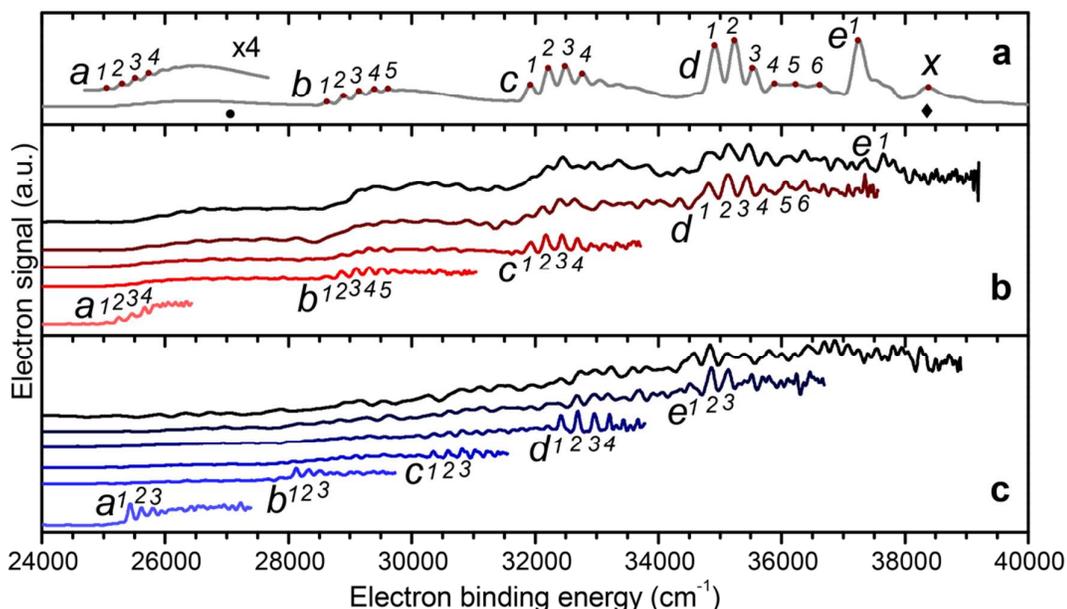
Figure 27. (a) Theoretical and (b) experimental photodetachment spectra of CH_3OHF^- showing transitions to resonances in the $F + CH_3OH \rightarrow HF + CH_3O$ product well, as well as (c) experimental photodetachment spectra of the CH_3ODF^- isotopolog. Experimental overview spectra are plotted in black and high-resolution traces taken at progressively lower photon energies are plotted in color. The ● and ♦ symbols represent the calculated product and reactant asymptotes, respectively. Reproduced from ref. 72 with permission from the Springer Nature, copyright 2017.
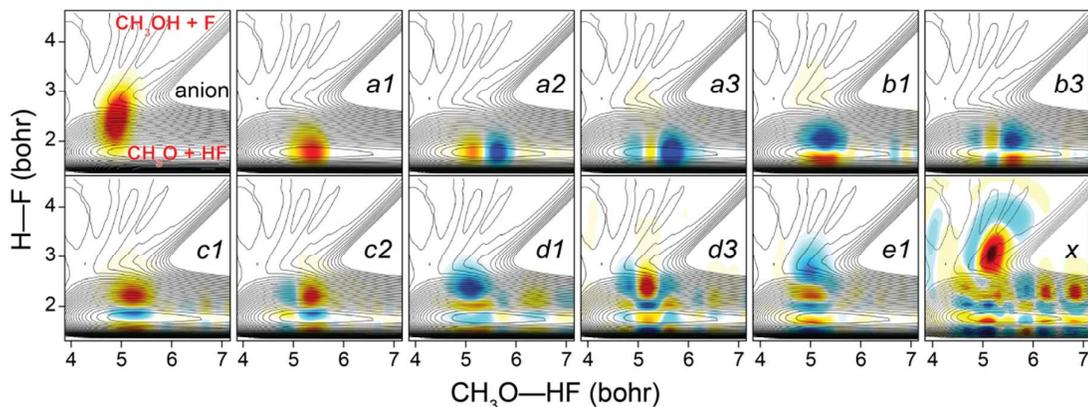
Figure 28. Cuts of the CH_3OHF^- anion vibrational ground state wavefunction and representative $F + CH_3OH \rightarrow HF + CH_3O$ resonance wavefunctions. The labels correspond to the related peaks in the simulated photodetachment spectrum of CH_3OHF^- (Fig. 23a). Wavefunctions are superimposed on the neutral PES contours plotted with respect to the CH_3O-HF and $H-F$ bond distances, while other four coordinates used in the quantum dynamical calculations are relaxed. Reproduced from ref. 72 with permission from the Springer Nature, copyright 2017.

References

[1] E. Fermi, *Nature, 1934,* 133, 757.

[2] E. Fermi, *Nature, 1934,* 133, 898-99.

[3] E. Fermi, E. Amaldi, O. D'Agostino, F. Rasetti, E. Segr´e, *Proc. Roy. Soc. London Ser. A,* 1934, 133, 483-500.

[4] E. Amaldi E, O. D'Agostino, E. Fermi, B. Pontecorvo, F. Rasetti, E. Segr´e, *Proc. R. Soc. London Ser. A, 1935,* 149, 522-58.

[5] H. A. Bethe, *Phys. Rev., 1935,* 47, 747-59.

[6] N. Bohr, *Nature, 1936,* 137, 344-48.

[7] P. Auger, *J. Phys. Radium, 1925,* 6, 205-8.

[8] R. Haas, *Z. Phys., 1957,* 148, 177-91.

[9] G. J. Schulz, *Phys. Rev., 1959,* 116, 1141-47.

[10] H. Eyring, M. Polanyi, *Z. fur Phys. Chem. B, 1931,* **12**, 279.

[11] H. Eyring, *J. Chem. Phys., 1935,* **3**, 107.

[12] M. G. Evans, M. Polanyi, *Trans. Faraday Soc.*, 1935, **31,** 875.

[13] J. C. Polanyi, A. H. Zewail, *Acc. Chem. Res., 1995,* **28**, 119-132.

[14] F. Fernandez-Alonso, R. N. Zare, *Annu. Rev. Phys. Chem.*, 2002, **53**, 67-99.

[15] R. S. Friedman, D. G. Truhlar, *Chem. Phys. Lett.,* 1991, **183**, 539-546.

[16] K. P. Liu, *Advances in Chemical Physics, 2012,* **149**, 1-46.

[17] S. D. Chao, R. T. Skodje, *Theor. Chem. Acc., 2002,* **108**, 273-285.

[18] X. Yang, *Annu. Rev. Phys. Chem., 2007,* **58**, 433-459.

[19] X. Yang, D. H. Zhang, *Acc. Chem. Res.* 2008, **41**, 981-989.

[20] C. Naulin, M. Costes, *Int. Rev. Phys. Chem.*, 2014, **33**, 427-446.

[21] K. P. Liu, *Annu. Rev. Phys. Chem.,* 2001, **52**, 139-164.

[22] H. Guo, *Int. Rev. Phys. Chem.,* 2012, **31**, 1-68.

[23] W. C. Lineberger, *Annu. Rev. Phys. Chem.,* 2013, **64**, 21-36.

[24] D. M. Neumark, *Phys. Chem. Chem. Phys.*, 2005, **7**, 433.

[25] R. B. Metz, A. Weaver, S. E. Bradforth, T. N. Kitsopoulos, and D. M. Neumark, *J. Phys. Chem.,* 1990, **94**, 1377-1388.

[26] S. E. Bradforth, A. Weaver, D. W. Arnold, R. B. Metz, and D. M. Neumark. *J. Chem. Phys.,* 1990, **92**, 7205.

[27] I. M. Waller, T. N. Kitsoupoulos, and D. M. Neumark, *J. Phys. Chem.,* 1990, **94**,

2240-2242.

[28] A. Osterwalder, M. J. Nee, J. Zhou, D. M. Neumark, *J. Chem. Phys.,* 2004, **121**, 6317-22.

[29] D. M. Neumark, *J. Phys. Chem. A*, 2008, **112**, 13287-301.

[30] C. Hock, J. B. Kim, M. L. Weichman, T. I. Yacovitch, D. M. Neumark, *J. Chem. Phys., 2012,* **137**, 244201.

[31] M. L. Weichman and D. M. Neumark, *Annu. Rev. Phys. Chem*. (in press)

[32] M. L. Weichman, et al. *PNAS*, 2016, **113**, 1698.

[33] Y. T. Lee, J. D. McDonald, P. R. LeBreton, and D. R. Herschbach, *Rev. Sci. Instrum.,* 1969, 40, 1402.

[34] M. J. Redmon, R. E. Wyatt, *Chem. Phys. Lett.*, 1979, 63,209-212.

[35] W. Dong, C. Xiao, T. Wang, D. Dai, X. Yang, D. H. Zhang, *Science,* 2010, **327**, 1501.

[36] X. Yang, D. Zhang, *Zeit. Phys. Chem.*, 2013, **227**, 1247-1265.

[37] L. Schnieder, W. Meier, K. H. Welge, M.N. R. Ashfold, C. M. Western, *J. Chem. Phys., 1990,* 92, 7027-37.

[38] L. Schnieder, K. Seekamp-Rahn, J. Borkowski, E. Wrede E, K. H. Welge, F. J. Aoiz, L. Banares, M. J. D'Mello, V. J. Herrero, V. Saez Rabanos, R. E. Wyatt, *Science, 1995,* 269, 207-10.

[39] L. Schnieder, K. Seekamp-Rahn, E. Wrede, K. H. Welge, *J. Chem. Phys.,* 1997, **107**, 6175-6195.

[40] B. R. Strazisar, C. Lin, H. F. Davis, *Science,* 2000, **290**, 958-961.

[41] M. Qiu, L. Che, Z. Ren, D. Dai, X. Wang, X. Yang, *Rev. Sci. Instrum.*, 2005, **76**, 083107.

[42] S. A. Harich, D. Dai, C. C. Wang, X. Yang, S. D. Chao, R. T. Skodje, *Nature, 2002,* **419**, 281.

[43] S. D. Chao, S. A. Harich, D. Dai, C. C. Wang, X. Yang, R. T. Skodje, *J. Chem. Phys.*, 2002, **117,** 8341-61.

[44] D. Dai D, C. C. Wang, S. A. Harich, X. Wang, X. Yang, S. D. Chao, R. T. Skodje, *Science, 2003,* **300**, 1730-3.

[45] J. Zhang, D. Dai, C. C. Wang, S. A. Harich, X. Wang, X. Yang, M. Gustaffson, R. T. Skodje, *Phys. Rev. Lett.*, 2006, **96**, 093201.

[46] S. -F. Wu, B. R. Johnson, R. D. Levine, *Mol. Phys.*, 1973, **25**, 839-856.

[47] G. C. Schatz, J. M. Bowman, A. Kuppermann, *J. Chem. Phys.*, 1973, **58**, 4023-4025.

[48] G. C. Schatz, J. M. Bowman, A. Kuppermann, *J. Chem. Phys.* 1975, **63**, 674-684.

[49] G. C. Schatz, J. M. Bowman, A. Kuppermann, *J. Chem. Phys.*, 1975, **63**, 685-696.

[50] D. M. Neumark, A. M. Wodtke, G. N. Robinson, C. C. Hayden, Y. T. Lee, *Phys. Rev. Lett., 1984,* **53**, 226.

[51] D. M. Neumark, A. M. Wodtke, G. N. Robinson, C. C. Hayden, Y. T. Lee, *J. Chem. Phys.,* 1985, **82**, 3045-3066.

[52] D. M. Neumark, A. M. Wodtke, G. N. Robinson, C. C. Hayden, K. Shobatake, R. K. Sparks, T. P. Schafer, Y. T. Lee, *J. Chem. Phys., 1985,* **82**, 3067-3077.

[53] F. J. Aoiz, L. Banares, V. J. Herrero, V. Saez Rabanos, K. Stark K, H. J. Werner, *Chem. Phys. Lett., 1994,* **223**, 215-226

[54] J. F. Castillo, D. E. Manolopoulos, K. Stark, H. J. Werner, *J. Chem. Phys., 1996,* **104**, 6531-6546.

[55] K. Stark, H. J. Werner, *J. Chem. Phys.*, 1996, **104**, 6515-6530.

[56] D. E. Manolopoulos, K. Stark, H. J. Werner, D. W. Arnold, S. E. Bradforth, D. M. Neumark, *Science*, 1993, **262**, 1852-1855.

[57] C. Hock, J. B. Kim, M. L. Weichman, T. I. Yacovitch, D. M. Neumark, *J. Chem. Phys., 2012,* **137**, 244201.

[58] R. T. Skodje, D. Skouteris, D. E. Manolopoulos, S.-H. Lee, F. Dong, K. Liu, *Phys. Rev. Lett.*, 2000, **85**, 1206.

[59] F. Dong, S. H. Lee, K. Liu, *J. Chem. Phys., 2000,* **113**, 3633-3640.

[60] R. T. Skodje, D. Skouteris, D. E. Manolopoulos, S. -H. Lee, F. Dong, K. Liu, *J. Chem. Phys.*, 2000, **112**, 4536-4552.

[61] S. D. Chao, R. T. Skodje, *J. Chem. Phys., 2000,* **113**, 3487-3491.

[62] M. Qiu, Z. Ren, L. Che, D. Dai, S. A. Harich, X.Wang, X. Yang, C. X. Xu, D. Xie, M. Gustafsson, R. T. Skodje, Z. Sun, D. H. Zhang, *Science, 2006,* **311**, 1440-1443.

[63] C. Xu, D. Xie, D. H. Zhang, *Chin. J. Chem. Phys., 2006,* **19**, 96-98.

[64] Z. Ren, L. Che, M. Qiu, X. Wang, W. Dong, D. Dai, X. Wang, X. Yang X, Z. Sun, B. Fu, S.-Y. Lee, X. Xu, D. H. Zhang, *Proc. Natl. Acad. Sci. U.S.A.*, 2008, **105**, 12662-12666.

[65] Z. Ren, Ph. D. Thesis, Dalian Institute of Chemical Physics, Chinese Academy of Sciences, Springer (2014).

[66] D. Yu, J. Chen, S. Cong, Z. Sun, *J. Phys. Chem. A,* 2015, **119**, 12193-12208.

[67] T. Wang, J. Chen, T. Yang, C. Xiao, Z. Sun, L. Huang, D. Dai, X. Yang, D. H. Zhang, *Science, 2013,* **342**, 1499-1502.

[68] T. Yang, J. Chen, L. Huang, T. Wang, C. Xiao, Z. Sun, D. Dai, X. Yang, D. H. Zhang, *Science*, 2015, **347**, 60-63.

[69] T. I. Yacovitch, E. Garand, J. B. Kim, C. Hock, T. Theis, D. M. Neumark, *Faraday Disc.*, **2012**, 157:399-414

[70] J. B. Kim, M. L. Weichman, T. F. Sjolander, D. M. Neumark, J. Klos et al., *Science*, 2015, **349**, 510-3.

[71] T. Westermann, J.B. Kim, M.L. Weichman, C. Hock, T.I. Yacovitch, J. Palma, D. M. Neumark, and U. Manthe, *Angew.Chemie. Int. Ed.,* 2014, **53**, 1122-1126.

[72] M.L. Weichman, J.A. Devine, M.C. Babin, J. Li, L.F. Guo, J.Y. Ma, H. Guo, and D.M. Neumark, *Nature Chem.,* 2017, **9**, 950-955.

[73] C. L. Russell, D. E. Manolopoulos, *Chem. Phys. Lett., 1996,* 256, 465-73.

[74] Jongjin B. Kim, Ph. D. Thesis, Department of Chemistry, University of California at Berkeley.

[75] F. Lique, G. L. Li, H. J. Werner, M. H. Alexander, *J. Chem. Phys.*, 2011, **134**, 231101.

[76] V. Aquilanti, S. Cavalli, D. De Fazio, A. Simoni, T. V. Tscherbul, *J. Chem. Phys.*, 2005, **123**, 054314.

[77] D. Sokolovski, S. K. Sen, V. Aquilanti, S. Cavalli, D. De Fazio, *J. Chem. Phys.*, 2007, **126**, 084305.

[78] X. Wang, W. Dong, M. Qiu, Z. Ren, L. Che, D. Dai, X. Wang, X. Yang, Z. Sun, B. Fu, S.-Y. Lee, X. Xu, D. H. Zhang, *Proc. Natl. Acad. Sci. U.S.A.*, 2008, **105**, 6227-6231.

[79] S. C. Althorpe, F. Fernandez-Alonso, B. D. Bean, J. D. Ayers, A. E. Pomerantz, R. N. Zare, E. Wrede, *Nature*, 2002, **416**, 67-70.

[80] S. A. Harich, D. Dai, C. Wang, X. Yang, S. D. Chao, R. T. Skodje, *Nature, 2002,* **419**, 281-284.

[81] D. E. Manolopoulos, *Nature, 2002,* **419**, 266-267.

[82] M. Lara, F. Dayou, J.-M. Launay, A. Bergeat, K. M. Hickson, C. Naulin, M. Costes, *Phys. Chem. Chem. Phys.,* 2011, **13**, 8127-8130.

[83] C. Berteloite, M. Lara, A. Bergeat, S. D. Le Picard, F. Dayou, K. M. Hickson, A.

Canosa, C. Naulin, J. M. Launay, I. R. Sims, M. Costes, *Phys. Rev. Lett.,* 2010*,* **105**, 203201.

84 V. Aquilanti, S. Cavalli, A. Simoni, A. Aguilar, J. M. Lucas, D. De Fazio, *J. Chem. Phys.*, 2004, **121**, 11675.

85 D. De Fazio, S. Cavalli, V. Aquilanti, A. A. Buchachenko, T. V. Tscherbul, *J. Phys. Chem. A*, 2007, **111**, 12538-12549.

86 D. Sokolovski, E. Akhmatskaya, C. Echeverría-Arrondo, D. De Fazio, *Phys. Chem. Chem. Phys.*, 2015, **17**, 18577-18589.

87 J. Chen, Z. Sun, D. H. Zhang, *J. Chem. Phys.,* 2015, **142**, 024303.

88 D. De Fazio, S. Cavalli, V. Aquilanti, *J. Phys. Chem. A*, 2016, **120**, 5288-5299.

89 W. Dong, C. Xiao, T. Wang, X. Yang, D. H. Zhang, *Science*, 2010, **327**, 1501-1502

90 J. C. Polanyi, *Acc. Chem. Res.,* 1972, **5**, 161-168

91 A. Sinha, M. C. Hsiao, F. F. Crim, *J. Chem. Phys., 1990,* **92**, 6333-6335.

92 F. F. Crim, Vibrational State Control of Bimolecular Reactions: Discovering and Directing the Chemistry. *Acc. Chem. Res.*, 1999, **32**, 877-884.

93 M. J. Bronikowski, W. R. Simpson, B. Girard B, R. N. Zare, *J. Chem. Phys.*, 1991, **95**, 8647-8648.

94 R. N. Zare, *Science, 1998,* **279**, 1875-1879.

95 F. Wang, K. P. Liu, *J. Phys. Chem. Lett.* 2011, **2**, 1421-1425.

96 S. Yan, Y. -T. Wu, B. Zhang, X.-F. Yue, K. Liu, *Science, 2007,* **316**, 1723-1726.

97 W. Zhang, H. Kawamata, K. P. Liu, *Science, 2009,* **325**, 303-306.

98 S. C. Althorpe, D. C. Clary, *Annu. Rev. Phys. Chem., 2003,* **54**, 493-529.

99 M. Alagia, N. Balucani, L. Cartechini, P. Casavecchia, E. H. van Kleef, G. G. Volpi, F. J. Aoiz, L. Banares, D. W. Schwenke, T. C. Allison, S. L. Mielke, D. G. Truhlar, *Science*, 1996, **273**, 1519-1522.

100 D. Skouteris, D. E. Manolopoulos, W. S. Bian, H. J. Werner, L. H. Lai, K. P. Liu, *Science*, 1999, **286**, 1713-1716.

101 D. Skouteris, H. J. Werner, F. J. Aoiz, L. Banares, J. F. Castillo, M. Menendez, N. Balucani, L. Cartechini, P. Casavecchia, *J. Chem. Phys.*, 2001, **114**, 10662-10672.

102 M. J. Ferguson, G. Meloni, H. Gomez, D. M. Neumark, *J. Chem. Phys.,* 2002, **117**, 8181-8184.

103 E. Garand, J. Zhou, D. E. Manolopoulos, M. H. Alexander, and D. M. Neumark, *Science,* 2008, **319**, 72-75.

[104] Z. Ren, L. Che, M. Qiu, X. Wang, D. Dai, S. A. Harich, X. Wang, X. Yang, C. Xu, D. Xie, Z. Sun, D. H. Zhang, *J. Chem. Phys.*, 2006, **125**, 151102.

[105] X. Liu, C. C. Wang, S. A. Harich, X. Yang, *Phys. Rev. Lett.*, 2002, **89**, 133201.

[106] J. Zhang, D. Dai, C. C. Wang, S. A. Harich, X. Wang, X. Yang, M. Gustafsson, R. T. Skodje, *Phys. Rev. Lett.,* 2006, **96**, 093201.

[107] W. Q. Zhang, H. Kawamata, and K. Liu, *Science*, 2009, **325**, 303-306.

[108] K. Liu, *Annu. Rev. Phys. Chem.,* 2016. **67**, 91–111.

[109] A.W. Ray, J. Agarwal, B.B, Shen, H. F. Schaefer, and R.E. Continetti, *Phys. Chem. Chem. Phys.,* 2016, **18**, 30612-30621.

[110] H. Feng, K. R. Randall, and H. F. Schaefer, *J. Phys. Chem. A,* 2015, 119, 1636–1641 (2015).

[111] S. E. Bradforth, D. W. Arnold, R. B. Metz, A. Weaver, D. M. Neumark, *J. Phys. Chem., 1991,* **95**, 8066-78.

[112] A. W. Ray, J. Agarwal, B. B. Shen, H. F. Schaefer, R. E. Continetti, *Phys. Chem. Chem. Phys.*, 2016, **18**, 30612-21.

[113] D. K. Bondi, J. N. L. Connor, J. Manz, and J. Romelt, *Mol. Phys*., 1983, **50**, 467-488.

[114] M. Lara, S. Chefdeville, K. M. Hickson, A. Bergeat, C. Naulin, J. M. Launay, M. Costes, *Phys. Rev. Lett., 2012,* **109**, 133201.

[115] C. Naulin, M. Costes, *Int. Rev. Phys. Chem.,* 2014, **33**, 427-446.

[116] S. Y. T. van de Meerakker, H. L. Bethlem, N. Vanhaecke, and G. Meijer, *Chem. Rev.*, 2012, **112**, 4828-4878.

[117] E. Narevicius and M. G. Raizen, *Chem. Rev.*, 2012, **112**, 4879-4889.

[118] M. Tizniti, S.D. Le Picard, F. Lique, C. Berteloite, A. Canosa, M.H. Alexander, and I.R. Sims, *Nature Chem.*, 2014, **6**, 141-145.